QUANTUM ALGORITHM DEVELOPMENT FOR ELECTRONIC STRUCTURE CALCULATIONS

by

Teng Bian

A Dissertation

Submitted to the Faculty of Purdue University

In Partial Fulfillment of the Requirements for the degree of

Doctor of Philosophy

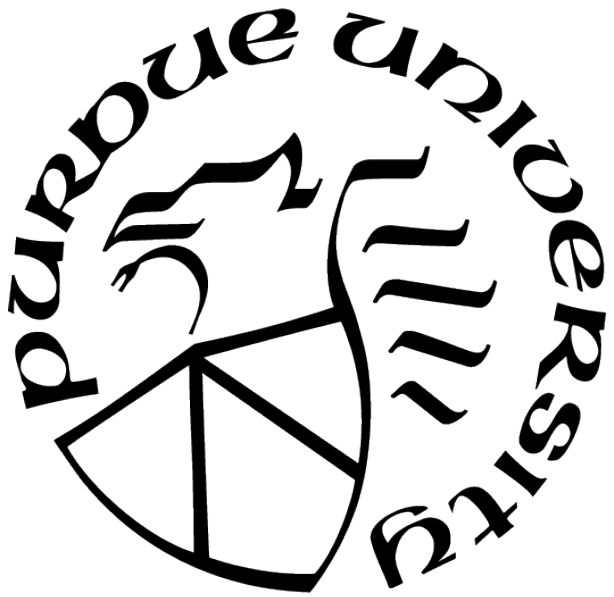

Department of Physics and Astronomy

West Lafayette, Indiana

December 2020

THE PURDUE UNIVERSITY GRADUATE SCHOOL
STATEMENT OF COMMITTEE APPROVAL

Dr. Sabre Kais, Chair

Department of Chemistry

Dr. Adam Wasserman

Department of Chemistry

Dr. Andreas Jung

Department of Physics and Astronomy

Dr. Arnab Banerjee

Department of Physics and Astronomy

Approved by:

Dr. John P. Finley

ACKNOWLEDGMENTS

I would like to express my sincere appreciation to my advisor Prof. Sabre Kais for his guidance, research advising, and consistent support during my pursuit of the Ph.D. degree. Also, I would like to thank the Kais Group members, especially Dr. Rongxin Xia and Dr. Zixuan Hu, for their kind and helpful discussions. I would like to thank Prof. Andrew Mugler and Prof. Y. Charlie Hu for advising me on research projects when taking their courses. I want to thank Prof. Adam Wasserman, Prof. Andreas Jung, and Prof. Arnab Banerjee for their time and efforts in being my committee members.

I would like to acknowledge the financial support from the Department of Physics and Chemistry at Purdue University, the Frederick N. Andrews Fellowship, Purdue Research Foundation, and the U.S. Department of Energy.

Finally, I want to thank my family and friends for their support and help for all these years.

TABLE OF CONTENTS

LIST OF TABLES

LIST OF FIGURES

ABBREVIATIONS

PEA	Phase Estimation Algorithm
VQE	Variational Quantum Eigensolver
FCVQE	Fully Controlled Variational Quantum Eigensolver

ABSTRACT

This dissertation concerns the development of quantum computing algorithms for solving electronic structure problems. Three projects are contained: comparison of quantum computing methods for the water molecule, the design and implementation of Fully Controlled Variational Quantum Eigensolver(FCVQE) method, and quantum computing for atomic and molecular resonances.

Chapter 1 gives a general introduction to quantum computing and electronic structure calculations. It includes basic concepts in quantum computing, such as quantum bits (qubits), quantum gates, and an important quantum algorithm, Phase Estimation Algorithm(PEA). It also shows the procedure of molecular Hamiltonian derivation for quantum computers.

Chapter 2 discusses several published quantum algorithms and original quantum algorithms to solve molecules' electronic structures, including the Trotter-PEA method, the first- and second-order Direct-PEA methods, Direct Measurement method, and pairwise Variational Quantum Eigensolver(VQE) method. These quantum algorithms are implemented into quantum circuits simulated by classical computers to solve the ground state energy and excited state energies of the water molecule. Detailed analysis is also given for each method's error and complexity.

Chapter 3 proposes an original design for VQE, which is called Fully Controlled Variational Quantum Eigensolver(FCVQE). Based on Givens Rotation matrices, this design constructs ansatz preparation circuits exploring all possible states in the given space. This method is applied to solving the ground state energy curves for different molecules, including NaH, H_2O, and N_2. The results from simulators turn out to be accurate compared with exact solutions. Gate complexity is discussed at the end of the chapter.

Chapter 4 attempts to apply quantum simulation to atomic and molecular resonances. The original design implements the molecule's resonance Hamiltonian into the quantum circuit, and the resonance properties can be obtained from the final measurement results. It is shown that the resonance energy and width of a model system can be calculated by executing the circuit using Qiskit simulators and IBM real quantum computers as well. A

proof of concept is also shown for the resonance properties of a real molecule, H_2^-. In the future, when there are more available qubits, longer coherence time, and less noise in quantum computers, this method can be used for larger molecular systems with better accuracy.

1. INTRODUCTION TO QUANTUM COMPUTING AND ELECTRONIC STRUCTURE CALCULATIONS

1.1 Overview

Electronic structure calculations are at the heart of quantum chemistry. It aims to figure out the properties of stationary states of many electrons that interact with each other under external potential and inner Coulomb repulsion. Solving electronic structures will significantly benefit physics- and chemistry-related fields, such as materials engineering and pharmaceutical development.

Electronic structure can be obtained by solving the Schrodinger equations for atoms, molecules, or extended systems. However, the determination of solutions is fundamentally hard for large systems. When the system size increases, the corresponding Hilbert space's dimensionality will increase exponentially, which makes the calculation soon exceed the current computers' computing power. Over the decades, many quantum chemistry methods have been put forward to solve the Schrodinger equation to chemical accuracy, 1 kcal/mole, such as ab initio, Density functional, Density Matrix, Algebraic, Quantum Monte Carlo, and Dimensional Scaling methods [1]–[4]. However, all of them encounter the computing resource escalation as the calculation pushes to either higher accuracy or larger systems. The computational complexity analysis [5]–[7] suggests this difficulty of quantum system simulation is inherent.

Quantum computing algorithms for electronic calculations provide a promising route to advance electronic structure calculations for large systems. Since quantum computers by nature have quantum mechanic properties such as entanglement and superposition, they have the potential to solve a system at a much lower cost of time than the simulations done by classical computers. The development and use of quantum computers for electronic structure calculations has the potential for revolutionary impact on the way of computation in the future[1].

In this thesis, I would like to leverage known or original quantum algorithms to solve molecular systems' electronic structure. To begin with, I will give an introduction to basic concepts of the most popular quantum computing model, the quantum circuit model. Then

I will elaborate how to transform an electronic structure calculation problem into a suitable problem for quantum computers. These two introductions will lay the foundation for my explorations into quantum computing methods for electronic structure calculations in later chapters.

1.2 Quantum Circuit

1.2.1 Quantum Bits

In classical computation, a bit is used as a basic unit of information, which is able to store a single binary value of 0 or 1. Quantum bit, or qubit, is an analogous concept in quantum computation. Similar to the classical case, qubit also has two basic states $|0\rangle$ and $|1\rangle$ corresponding to 0 and 1. The difference is that, a qubit can also store the superposition of these two states, like:

$$|\psi\rangle = \alpha\,|0\rangle + \beta\,|1\rangle\,, \tag{1.1}$$

or in the vector form:

$$|\psi\rangle = \begin{pmatrix} \alpha \\ \beta \end{pmatrix}. \tag{1.2}$$

In the above two representations, α and β are two complex numbers that satisfy the normalization condition: $|\alpha|^2 + |\beta|^2 = 1$. Classical bits are determined to be measured in the state 0 or 1. However, for a qubit like the above $|\psi\rangle$, because of quantum mechanic effects, when doing measurement, it will collapse into either $|0\rangle$ or $|1\rangle$ with probability $|\alpha|^2$ or $|\beta|^2$. The power of superposition and the problem of measurement for qubits makes it behave different from bits.

Multiple bits can be used to represent a binary number of multiple digits. For example, 2 bits are able to store 4 possible states: 00, 01, 10 and 11. Correspondingly, a pair of qubits will represent a superposition of 4 quantum basis sates, like

$$|\psi\rangle = \alpha_{00}|00\rangle + \alpha_{01}|01\rangle + \alpha_{10}|10\rangle + \alpha_{11}|11\rangle, \tag{1.3}$$

where $|\alpha_{ij}|^2$ gives the probability of getting state $|ij\rangle$ after measurement and satisfies the normalization condition. If only one qubit is measured, for example the first qubit, the measurement result will be 0 or 1 with probability $\frac{\sqrt{|\alpha_{00}|^2+|\alpha_{01}|^2}}{\sqrt{|\alpha_{00}|^2+|\alpha_{01}|^2+|\alpha_{10}|^2+|\alpha_{11}|^2}}$ or $\frac{\sqrt{|\alpha_{10}|^2+|\alpha_{11}|^2}}{\sqrt{|\alpha_{00}|^2+|\alpha_{01}|^2+|\alpha_{10}|^2+|\alpha_{11}|^2}}$, while the qubits' state after measurement will be respectively

$$|\psi\rangle = \frac{\alpha_{00}|00\rangle + \alpha_{01}|01\rangle}{\sqrt{|\alpha_{00}|^2+|\alpha_{01}|^2}} \quad \text{or} \quad |\psi\rangle = \frac{\alpha_{10}|10\rangle + \alpha_{11}|11\rangle}{\sqrt{|\alpha_{10}|^2+|\alpha_{11}|^2}}. \tag{1.4}$$

Similarly, a n-qubit register can store a superposition of 2^n basis states and will collapse when measured.

1.2.2 Quantum Gates

There are elementary logic gates in classical computation, including AND, OR, XOR, NOT, etc., that can manipulate bits' states based on Boolean algebra. In quantum computation, quantum gates are used for similar purposes. The analogous quantum gate for NOT gate is called X gate and can be used to flip the qubit state between $|0\rangle$ and $|1\rangle$, which has matrix form:

$$X \equiv \begin{pmatrix} 0 & 1 \\ 1 & 0 \end{pmatrix}. \tag{1.5}$$

Applying X gate to the single-qubit state $|\psi\rangle$leads to

$$X|\psi\rangle = \begin{pmatrix} 0 & 1 \\ 1 & 0 \end{pmatrix} \begin{pmatrix} \alpha \\ \beta \end{pmatrix} = \begin{pmatrix} \beta \\ \alpha \end{pmatrix}. \tag{1.6}$$

This X gate is very much like Pauli matrix σ_x. There are also Y gate and Z gate similar to Pauli matrices σ_y and σ_z as follows:

$$Y \equiv \begin{pmatrix} 0 & -\mathrm{i} \\ \mathrm{i} & 0 \end{pmatrix}, Z \equiv \begin{pmatrix} 1 & 0 \\ 0 & -1 \end{pmatrix}. \tag{1.7}$$

Hadamard gate H is also very useful in algorithm implementations:

$$H \equiv \frac{1}{\sqrt{2}} \begin{pmatrix} 1 & 1 \\ 1 & -1 \end{pmatrix}. \tag{1.8}$$

Other useful operators for one-qubit manipulation includes three rotational operators $R_x(\theta)$, $R_y(\theta)$ and $R_z(\theta)$:

$$R_x(\theta) \equiv \mathrm{e}^{-\mathrm{i}\theta X/2} = \cos\frac{\theta}{2} I - \mathrm{i}\sin\frac{\theta}{2} X = \begin{pmatrix} \cos\frac{\theta}{2} & -\mathrm{i}\sin\frac{\theta}{2} \\ -\mathrm{i}\sin\frac{\theta}{2} & \cos\frac{\theta}{2} \end{pmatrix}, \tag{1.9}$$

$$R_y(\theta) \equiv \mathrm{e}^{-\mathrm{i}\theta Y/2} = \cos\frac{\theta}{2} I - \mathrm{i}\sin\frac{\theta}{2} Y = \begin{pmatrix} \cos\frac{\theta}{2} & -\sin\frac{\theta}{2} \\ \sin\frac{\theta}{2} & \cos\frac{\theta}{2} \end{pmatrix}, \tag{1.10}$$

$$R_z(\theta) \equiv \mathrm{e}^{-\mathrm{i}\theta Z/2} = \cos\frac{\theta}{2} I - \mathrm{i}\sin\frac{\theta}{2} Z = \begin{pmatrix} \mathrm{e}^{-\mathrm{i}\theta/2} & 0 \\ 0 & \mathrm{e}^{\mathrm{i}\theta/2} \end{pmatrix}. \tag{1.11}$$

Here I in the formulas is a two-by-two identity matrix. Any unitary operation U can be decomposed into a phase and two of the above rotational operations[8]. For instance,

$$\begin{aligned} U &= \mathrm{e}^{\mathrm{i}\alpha} R_z(\beta) R_y(\gamma) R_z(\delta) \\ &= \begin{pmatrix} \mathrm{e}^{\mathrm{i}(\alpha-\beta/2-\delta/2)}\cos\frac{\gamma}{2} & -\mathrm{e}^{\mathrm{i}(\alpha-\beta/2+\delta/2)}\sin\frac{\gamma}{2} \\ \mathrm{e}^{\mathrm{i}(\alpha+\beta/2-\delta/2)}\sin\frac{\gamma}{2} & \mathrm{e}^{\mathrm{i}(\alpha+\beta/2+\delta/2)}\cos\frac{\gamma}{2} \end{pmatrix} \end{aligned} \tag{1.12}$$

To entangle different qubits' states together, controlled operations are introduced. The primary one is controlled-NOT gate, or CNOT gate. In a two-qubit register, using the first qubit to control the second one has the following matrix representation:

$$CNOT = \begin{pmatrix} 1 & 0 & 0 & 0 \\ 0 & 1 & 0 & 0 \\ 0 & 0 & 0 & 1 \\ 0 & 0 & 1 & 0 \end{pmatrix}, \tag{1.13}$$

with circuit representation as Figure 1.1. For an arbitrary gate U, the general control

Figure 1.1. Quantum circuit representation of CNOT gate.

operation, known as controlled-U, can be expressed as

$$[hbt!]\text{controlled-}U = \begin{pmatrix} 1 & 0 & 1 & 0 \\ 0 & 1 & 0 & 1 \\ 1 & 0 & & \\ 0 & 1 & & U \end{pmatrix}, \tag{1.14}$$

with circuit representation as Figure 1.2. There are also multi-controlled qubit gates, like Toffoli gate, which has two control qubits and one target qubit. The circuit representation is shown as in Figure 1.3. This gate can be implemented by single-qubit gates and $CNOT$ gates. It can also be a building block for other multi-controlled gates. For example, a 3-controlled NOT gate is equal to 3 Toffoli gates when an extra ancilla qubit is available,

Figure 1.2. Quantum circuit representation of controlled-U gate.

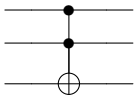

Figure 1.3. Quantum circuit representation of Toffoli gate.

as shown in Figure 1.4. Similarly, a 3-controlled U gate is equal to two Toffoli and one 2-controlled U gate. The 2-controlled U gate can be further decomposed as shown in Figure 1.5, where $U = V^2$.

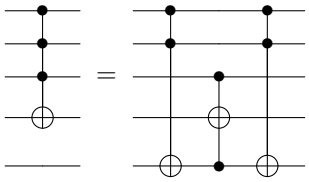

Figure 1.4. Decomposition of 3-controlled NOT gate into Toffoli gates.

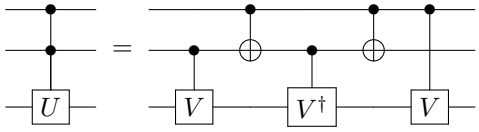

Figure 1.5. Decomposition of 2-controlled U gate into controlled gates.

1.2.3 Phase Estimated Algorithm

One of the most important algorithms for quantum chemistry is Phase Estimation Algorithm(PEA)[9], [10]. PEA can be used to solve the phase of some operator's eigenvalue. Suppose a unitary operator U has an eigenvector $|u\rangle$ with corresponding eigenvalue $e^{2\pi i\varphi}$, i.e. $U|u\rangle = e^{2\pi i\varphi}|u\rangle$. PEA can estimate the value of φ via the process of preparing the state $|u\rangle$, applying the Hadamard gates and the controlled-U operations, performing the inverse Fourier transformation, and doing the final measurements.

Assume that the input state $|0\rangle|u\rangle$ has been prepared, in which $|0\rangle$ is an ancillary qubit's state. After applying a Hadamard gate to the ancillary qubit, and then a controlled-$U^{2^{\mathrm{j}}}$ gate to the whole system, the output state would be

$$\frac{|0\rangle + \mathrm{e}^{2\pi\mathrm{i}(2^{\mathrm{j}}\varphi)}|1\rangle}{\sqrt{2}}|u\rangle\,. \tag{1.15}$$

If φ has a binary estimation of $0.\varphi_1\varphi_2...\varphi_t$, by introducing t ancillary qubits and applying controlled-$U^{2^{t-\mathrm{j}-1}}$ operation on each j^{th} qubit, the output state would be

$$\begin{aligned}&\frac{|0\rangle + \mathrm{e}^{2\pi\mathrm{i}(2^{t-1}\varphi)}|1\rangle}{\sqrt{2}}\cdots\frac{|0\rangle + \mathrm{e}^{2\pi\mathrm{i}(2^{1}\varphi)}|1\rangle}{\sqrt{2}}\frac{|0\rangle + \mathrm{e}^{2\pi\mathrm{i}(2^{0}\varphi)}|1\rangle}{\sqrt{2}}|u\rangle\\ =&\frac{|0\rangle + \mathrm{e}^{2\pi\mathrm{i}0.\varphi_t}|1\rangle}{\sqrt{2}}\cdots\frac{|0\rangle + \mathrm{e}^{2\pi\mathrm{i}0.\varphi_2...\varphi_t}|1\rangle}{\sqrt{2}}\frac{|0\rangle + \mathrm{e}^{2\pi\mathrm{i}0.\varphi_1\varphi_2...\varphi_t}|1\rangle}{\sqrt{2}}|u\rangle\end{aligned} \tag{1.16}$$

This form is very much like the outcome of quantum Fourier transformation:

$$|\mathrm{j}_1\mathrm{j}_2...\mathrm{j}_t\rangle \rightarrow \frac{(|0\rangle + \mathrm{e}^{2\pi\mathrm{i}0.\mathrm{j}_t}|1\rangle)(|0\rangle + \mathrm{e}^{2\pi\mathrm{i}0.\mathrm{j}_2\cdots\mathrm{j}_t})\cdots(|0\rangle + \mathrm{e}^{2\pi\mathrm{i}0.\mathrm{j}_1\cdots\mathrm{j}_t}|1\rangle)}{2^{t/2}} \tag{1.17}$$

In this way, by performing the inverse quantum Fourier transformation, we can get the output state $|\varphi_1\varphi_2...\varphi_t\rangle$ and obtain $\varphi \approx 0.\varphi_1\varphi_2...\varphi_t$ by measurements.

1.3 Molecular Hamiltonian Derivation for Quantum Computers

The time-independent Schrödinger Equation for a molecular system is

$$H_{mol}|\psi\rangle = E|\psi\rangle\,, \tag{1.18}$$

where H_{mol} is the molecular Hamiltonian, $|\psi\rangle$ is a multi-particle eigenstate of the molecular system, and E is the corresponding eigenenergy. In Born-Oppenheimer approximation(BOA), nuclei can be treated as stationary point charges. In this way, the molecular Hamiltonian can be simplified as

$$H = -\sum_{\mathrm{i}}\frac{1}{2}\nabla_{\mathrm{i}}^2 - \sum_{\sigma}\sum_{\mathrm{i}}\frac{Z_\sigma}{|\vec{r}_{\mathrm{i}} - \vec{R}_\sigma|} + \sum_{\mathrm{i}}\sum_{\mathrm{j}>\mathrm{i}}\frac{1}{r_{\mathrm{ij}}}. \tag{1.19}$$

Here Z_σ is the σ^{th} nuclear charge, $\vec{r}_\mathrm{i}$ is the position of electron i, r_ij is the distance between the two points r_i and r_j, and $\vec{R}_\sigma$ is the position of σ^{th} nucleus. To solve the electronic structures of this Hamiltonian by quantum computer, we need to transform it into the form of Pauli matrices

$$H = \sum_\mathrm{i} h_\mathrm{i} P_\mathrm{i}. \tag{1.20}$$

Here h_i is some coefficient and P_i is a tensor product of Pauli matrices X, Y, Z and 2-by-2 identity matrix I. The detailed steps for transformation are shown in the following subsections.

1.3.1 Second Quantization

After selecting basis functions for the molecular system, its Hamiltonian can be expressed in the second quantization form[4], [11], [12]

$$H = \sum_{\mathrm{i,j}} h_\mathrm{ij} a_\mathrm{i}^\dagger a_\mathrm{j} + \frac{1}{2} \sum_{\mathrm{i,j},k,l} h_{\mathrm{ij}kl} a_\mathrm{i}^\dagger a_\mathrm{j}^\dagger a_k a_l, \tag{1.21}$$

Here $a_\mathrm{i}^\dagger$ and a_i are fermionic creation and annihilation operators, and $h_\mathrm{i,j}$ and $h_{\mathrm{i,j},k,l}$ are coefficients for one-body and two-body interactions. These coefficients can be calculated by the following expressions:

$$\begin{aligned} h_\mathrm{ij} &= \int d\vec{r}_1 \chi_\mathrm{i}^*(\vec{r}_1)(-\frac{1}{2}\nabla_1^2 - \sum_\sigma \frac{Z_\sigma}{|\vec{r}_1 - \vec{R}_\sigma|})\chi_\mathrm{j}(\vec{r}_1), \\ h_{\mathrm{ij}kl} &= \int d\vec{r}_1 d\vec{r}_2 \chi_\mathrm{i}^*(\vec{r}_1)\chi_\mathrm{j}^*(\vec{r}_2)\frac{1}{r_{12}}\chi_k(\vec{r}_2)\chi_l(\vec{r}_1). \end{aligned} \tag{1.22}$$

Here $\chi_\mathrm{i}(\vec{r})$ is the i^{th} spin orbital in the basis function set.

1.3.2 Mapping from Fermionic Systems to Qubit Systems

The fermionic Hamiltonian in the second quantization form is not suitable for quantum computers yet. We still need to transform this Hamiltonian into the Hamiltonian of the Pauli matrix form. There are mainly three transformations to build the mapping.

The first transformation, also the most well-known one, is Jordan-Wigner transformation[13]. The fermionic creation and annihilation operators will be replaced respectively by Pauli matrices[11]

$$a_{\mathrm{j}}^{\dagger} = \frac{1}{2}(X_{\mathrm{j}} - \mathrm{i}Y_{\mathrm{j}}) \otimes Z_{\mathrm{j-1}}^{\rightarrow}, \tag{1.23}$$

$$a_{\mathrm{j}} = \frac{1}{2}(X_{\mathrm{j}} + \mathrm{i}Y_{\mathrm{j}}) \otimes Z_{\mathrm{j-1}}^{\rightarrow}, \tag{1.24}$$

where

$$Z_{\mathrm{j-1}}^{\rightarrow} \equiv Z_{\mathrm{j-1}} \otimes Z_{\mathrm{j-2}} \otimes \cdots \otimes Z_1 \otimes Z_0. \tag{1.25}$$

Note that for simplicity, the identity operator is omitted in tensor products when a qubit is not operated by any Pauli matrix. In this Hamiltonian transformation, the fermionic state and the qubit state would be exactly the same:

$$\begin{gathered} |f_{n-1}f_{n-2}...f_1f_0\rangle \rightarrow |q_{n-1}q_{n-2}...q_1q_0\rangle\,, \\ q_{\mathrm{i}} = f_{\mathrm{i}} \in \{0,1\}. \end{gathered} \tag{1.26}$$

Here f_{i} represents the occupation number of the i^{th} spin-orbital, q_{i} represents the state of the i^{th} qubit, and n is the number of spin orbitals.

The second transformation is based on the parity basis encoding[11], [14]. Rather than store the occupancy number of the i^{th} spin-orbital, now qubit q_{i} is used to store the parity of all occupied spin-orbitals up to i^{th} spin-orbital, i.e.

$$q_{\mathrm{i}} = \sum_{k=0}^{\mathrm{i}} f_k \bmod 2 \in \{0,1\}. \tag{1.27}$$

The mapping from fermionic creation and annihilation operators becomes

$$a_{\mathrm{j}}^{\dagger} = X_{\mathrm{j+1}}^{\leftarrow} \otimes \frac{1}{2}(X_{\mathrm{j}} \otimes Z_{\mathrm{j-1}} - \mathrm{i}Y_{\mathrm{j}}), \tag{1.28}$$

$$a_{\mathrm{j}} = X_{\mathrm{j+1}}^{\leftarrow} \otimes \frac{1}{2}(X_{\mathrm{j}} \otimes Z_{\mathrm{j-1}} + \mathrm{i}Y_{\mathrm{j}}), \tag{1.29}$$

where

$$X_{\mathrm{j}+1}^{\leftarrow} \equiv X_{n-1} \otimes X_{n-2} \otimes \cdots \otimes X_{\mathrm{j}+2} \otimes X_{\mathrm{j}+1}. \tag{1.30}$$

The third one is called Bravyi-Kitaev transformation[14]. It is kind of a variant of parity basis transformation, while the difference is that each qubit stores the parity of a specially designed part of spin-orbitals' occupancy numbers.

After any of the above transformation, the molecular Hamiltonian can be written in Pauli matrix form

$$H = \sum_{\mathrm{i}} h_{\mathrm{i}} P_{\mathrm{i}}, \tag{1.31}$$

which can be used for quantum algorithms. One thing worth to be mentioned is that, if expanded in $2^n \times 2^n$ matrix form, the Hamiltonian for molecules will always be real and symmetric because h_{ij}, $h_{\mathrm{ij}kl}$ are real, and $a_{\mathrm{j}}^{\dagger}$, a_{j} are real matrices.

2. COMPARISON OF QUANTUM COMPUTING METHODS FOR THE WATER MOLECULE

2.1 Introduction

In 1982, Feynman proposed to calculate a large quantum system by precisely control some smaller quantum system[15]. He claimed that we are able to create an analogy to some quantum system, if we have enough control over the states of some other quantum system. In the previous chapter we also created analogies: by Jordan-Wigner/Parity/Bravyi-Kitaev transformation [13], [14], we mapped an electronic structure Hamiltonian to a Hamiltonian of Pauli matrix form, which preserves energy eigenvalues [16]. Then the evolution under original Hamiltonian, e^{-iHt}, can be approximately simulated on quantum computers. This quantum simulation process may serve as a potentially efficient method to calculate eigenenergies of a given molecule. Classically, the computational cost of this problem grows exponentially with the system size, n, the number of orbital basis functions[17]. However, using phase estimation algorithm(PEA) [9], [18], molecule's ground state energies can be calculated with gate depth $O(poly(n))$ [19]–[21].

The most general way to approximately implement the propagator, e^{-iHt}, is through a Trotter-Suzuki decomposition[22]–[24]. Also, it is shown that the Hamiltonian dynamics can be simulated through a truncated Taylor series [25], which is generalized as quantum signal processing[26]. Recently, a direct circuit implementation of the Hamiltonian combined with phase estimation algorithm (Direct-PEA) is also proposed [27]–[29]: the designed circuit approximates the time evolution operator by using the truncated series such as $U = I - \frac{iH}{\kappa}$ and $U = tH + i(I - \frac{t^2H^2}{2})$, in which κ and t are parameters to restrict truncation error. Then these unitary operators can be used to calculate ground state energies of Hamiltonians. Recently an approach called Variational Quantum Eigensolver (VQE) method has been introduced by Aspuru-Guzik etal [30], [31], which is a hybrid quantum-classical algorithm and will significantly reduce the gate complexity at the cost of a large amount of measurements. It has also been applied on real-world quantum computers to obtain ground state energies of molecules such as H_2, LiH and BeH_2 [32], [33].

This chapter explores all the above methods to calculate the ground state energy curve of the water molecule[34]. In the beginning, the way to reduce the number of qubits required for simulation is illustrated. Then, it discusses five methods of electronic structure simulation on quantum computers: a phase estimation method using first order Trotter-Suzuki decomposed propagator (Trotter-PEA), two direct implementations of the Hamiltonian of Pauli matrix form (Direct-PEA), a direct measurement method and a specific VQE method(Pairwise VQE). Each method gives the circuit design, error and complexity analysis and the simulation results: a ground state energy curve. At the end of this chapter, all the method's accuracy and gate complexity are compared.

2.2 Qubit Reduction for Water Molecule

Implementing quantum algorithms either in a quantum computer or in a simulated classical computer is very time-consuming and space-consuming when qubit number is large. For molecular systems like water molecule, we can take advantage of symmetry properties and do qubit reduction in advance [33], [35].

Taking STO-3G basis set for water molecule, the $1s$ orbitals of each hydrogen atom along with the $1s$, $2s$, $2p_x$, $2p_y$ and $2p_z$ orbitals for oxygen atom need to be considered. Considering spin, there are a total of 14 molecular orbitals. Assuming that the two molecular orbitals of the largest energies are vacant, the Hamiltonian after second quantization can then be expressed as

$$H = \sum_{\mathrm{i,j}=1}^{12} h_{\mathrm{ij}} a_{\mathrm{i}}^{\dagger} a_{\mathrm{j}} + \frac{1}{2} \sum_{\mathrm{i,j},k,l=1}^{12} h_{\mathrm{ij}kl} a_{\mathrm{i}}^{\dagger} a_{\mathrm{j}}^{\dagger} a_k a_l. \tag{2.1}$$

Here h_{ij} and $h_{\mathrm{ij}kl}$ are calculated by Eq. (1.21). The molecular orbitals are ordered from 1 to 12 as $\{1\uparrow, 2\uparrow ..., 6\uparrow, 1\downarrow, 2\downarrow, ...6\downarrow\}$, in which spin-up orbitals are ordered from lowest to highest energy and then spin-down orbitals the same. Group the 4 lowest energy spin-orbital $\{1\uparrow, 2\uparrow, 1\downarrow, 2\downarrow\}$ into the set $F = \{1, 2, 7, 8\}$ and assume that for the ground state of water

molecule, the spin-orbitals in the set F will be filled with electrons. Then some one-body and two-body electron interaction terms can be simplified in the following ways:

$$\begin{aligned} &a_1^\dagger a_1 = 1, \quad a_2^\dagger a_2 = 1, \quad a_7^\dagger a_7 = 1, \quad a_8^\dagger a_8 = 1, \\ &a_{\mathrm{i}}^\dagger a_{\mathrm{j}} = 0, \text{ if i} \neq \text{j , and i} \in F \text{ or } \text{ j} \in F, \end{aligned} \tag{2.2}$$

$$a_{\mathrm{i}}^\dagger a_{\mathrm{j}}^\dagger a_k a_l = \begin{cases} a_{\mathrm{j}}^\dagger a_k, & \mathrm{i} = l, \mathrm{i} \in F, \{\mathrm{j}, k\} \notin F, \\ a_{\mathrm{i}}^\dagger a_l, & \mathrm{j} = k, \mathrm{j} \in F, \{\mathrm{i}, l\} \notin F, \\ -a_{\mathrm{j}}^\dagger a_l, & \mathrm{i} = k, \mathrm{i} \in F, \{\mathrm{j}, l\} \notin F, \\ -a_{\mathrm{i}}^\dagger a_k, & \mathrm{j} = l, \mathrm{j} \in F, \{\mathrm{i}, k\} \notin F. \end{cases} \tag{2.3}$$

The above simplification along with the ability to neglect two-body operators that contains an odd numbers of modes in F restricts spin-orbitals to a new set $\{3\uparrow, 4\uparrow, 5\uparrow, 6\uparrow, 3\downarrow, 4\downarrow, 5\downarrow, 6\downarrow\}$. After relabelling the orbital set 1 to 8 and doing parity basis transformation, the fermionic Hamiltonian can be mapped into an 8-local Hamiltonian representated by tensor products of Pauli matrices: $H = \sum_{\mathrm{i}} h_{\mathrm{i}} P_{\mathrm{i}}$. The mapping of states is

$$\begin{aligned} |f_{n-1} f_{n-2} ... f_1 f_0\rangle \rightarrow |q_{n-1} q_{n-2} ... q_1 q_0\rangle \,, \\ q_{\mathrm{i}} = \sum_{k=0}^{\mathrm{i}} f_k \bmod 2 \in \{0, 1\}. \end{aligned} \tag{2.4}$$

Assuming that in the ground state of water molecule, half of the left 6 electrons are spin-up while the other half are spin-down. The parity value in q_4 and q_8 are determined to be $|1\rangle$ and $|0\rangle$ respectively. This means only Z_4, I_4, Z_8, I_8 will act on q_4 and q_8. Since $Z_4 |q_4\rangle = -|q_4\rangle$ and $Z_8 |q_8\rangle = |q_8\rangle$, Z_4 and Z_8 can be substituted by $-I_4$ and I_8 respectively, which reduces the Hamiltonian to a 6-local one. From now on,

$$H = \sum_{\mathrm{i}=1}^{L} \alpha_{\mathrm{i}} h_{\mathrm{i}} \tag{2.5}$$

will be to represent this reduced 6-local Hamiltonian. Here $\{\alpha_{\mathrm{i}}\}$ are coefficients and $\{h_{\mathrm{i}}\}$ are tensor products of Pauli matrices $\{X_{\mathrm{i}}, Y_{\mathrm{i}}, Z_{\mathrm{i}}\}$ and identity matrix I_{i}. This Hamiltonian will

be used for method in the following sections to solve electronic structure problems. As an example, water molecule's Hamiltonian at O-H bond length 1.9 a.u. is shown in Appendix A.1.

For other molecules, a similar process can also be applied to obtain a new Hamiltonian with reduced qubit requirement.

2.3 Trotter-PEA Method

2.3.1 The Procedure of the Method

For each h_i in the Hamiltonian H, the operator $\mathrm{e}^{-\mathrm{i}\alpha_\mathrm{i}h_\mathrm{i}t}$ can be easily implemented into quantum circuit. Since h_i doesn't commute with each other for most cases, generally the propagator $\mathrm{e}^{-\mathrm{i}Ht}$ can not be implemented term by term, i.e. $\mathrm{e}^{-\mathrm{i}Ht} \neq \prod_{\mathrm{i}=1}^{L} \mathrm{e}^{-\mathrm{i}\alpha_\mathrm{i}h_\mathrm{i}t}$. However, it can still be a good approximation for a small t, according to the first-order Trotter-Suzuki decomposition

$$U = \prod_{\mathrm{i}=1}^{L} \mathrm{e}^{-\mathrm{i}\alpha_\mathrm{i}h_\mathrm{i}t} = \mathrm{e}^{-\mathrm{i}Ht} + O(A^2t^2). \tag{2.6}$$

In the above equation, A is defined as the sum of the absolute value of coefficients: $A = \sum_{\mathrm{i}=1}^{L} |\alpha_\mathrm{i}|$, and the error of approximate is $O(A^2t^2)$ for a small time t. Note that Eq. (2.6) is a bit different from original Trotter-Suzuki decomposition, for here t can be adjust as small as necessary for error control. The U operator is very easy to implement on the state register since it only requires a sequence of multi-qubit rotations.

The unitary operator U can be utilized in PEA to extract the energy from the phase. Using extra ancilla qubits, desired accuracy is able to be achieved by iterative measurements[19], [36], [37]. This PEA based on the first order Trotter-Suzuki decomposition is called Trotter-PEA in this work. Although higher order Trotter-Suzuki decompositions are available, their form are more complicated, especially for order higher than 2. In this way, only first order case is discussed here for simplicity.

A forward iterative PEA[29] that estimates the phase from the most significant bit is used in the simulation to reduce required qubits. It only needs 1 qubit for measurement as

shown in Figure 2.1. Assuming the input state $|\psi\rangle_s$ is the ground state of H, the state before the measurement operation would be

$$\frac{1+e^{i2\pi(0.\phi_{k+1}\phi_{k+2}\ldots-0.01)}}{2}e^{i\frac{\pi}{4}}|0\rangle|\psi\rangle_s+\frac{1-e^{i2\pi(0.\phi_{k+1}\phi_{k+2}\ldots-0.01)}}{2}e^{i\frac{\pi}{4}}|1\rangle|\psi\rangle_s. \tag{2.7}$$

If the measurement qubit has a greater probability of output state $|1\rangle$, $\phi_{k+1}=1$. Otherwise $\phi_{k+1}=0$. The ground state energy can be calculated by $E=-2\pi\times 0.\phi_1\phi_2\phi_3\cdots$. The energy curve of water molecule is shown in Figure 2.2.

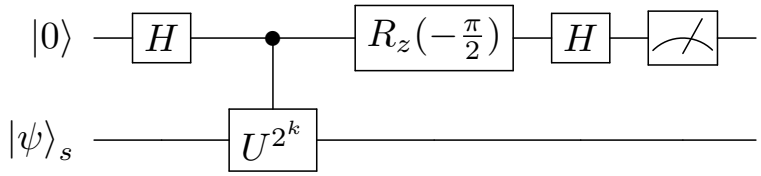

Figure 2.1. Forward iterative PEA circuit with initial state $|0\rangle|\psi\rangle_s$. Here $|\psi\rangle_s$ is the ground state of the Hamiltonian, H is the Hadamard gate, U is the approximate propagator and $R_z(-\frac{\pi}{2})$ is a Z rotation gate.

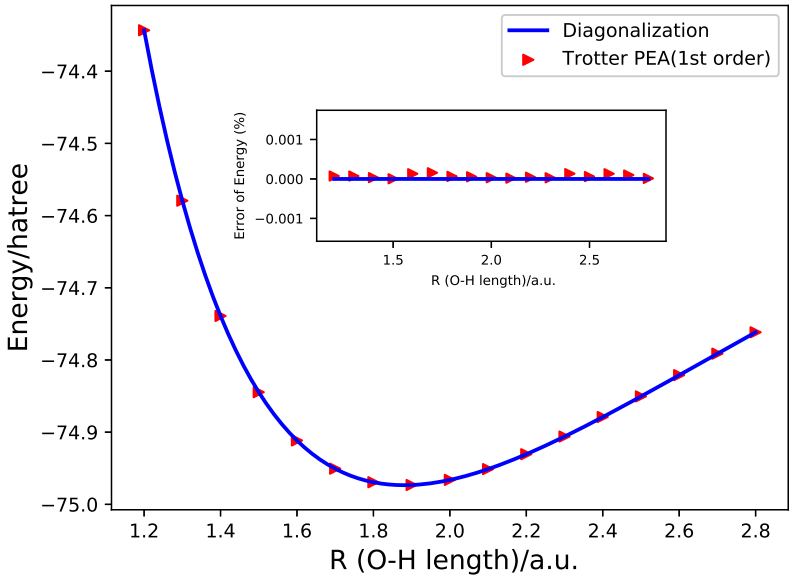

Figure 2.2. Ground State Energy Curve for H_2O, as a function of the bond length O-H in a.u. for Trotter-PEA. Errors are shown in the window of the figure.

2.3.2 Error Analysis

Based on Eq. 2.6, the state after performing U operator can be represented by

$$\begin{aligned}\prod_{\mathrm{i}=1}^{L} \mathrm{e}^{-\mathrm{i}\alpha_\mathrm{i} h_\mathrm{i} t} \left|\psi\right\rangle_s &= (\mathrm{e}^{-\mathrm{i}Ht} - O(A^2t^2) \left|\psi\right\rangle_s \\ &= (1 - O(A^2t^2))\mathrm{e}^{-\mathrm{i}(Et+O(A^2t^2)} \left|\psi\right\rangle_s + O(A^2t^2) \left|\psi^\perp\right\rangle . \end{aligned} \tag{2.8}$$

In the above equation $\left|\psi^\perp\right\rangle$ is a state perpendicular to $\left|\psi\right\rangle_s$. Note that, $O(A^2t^2)$ is an operator before it's applied to $\left|\psi\right\rangle_s$, and is a number afterwards. From Eq. (2.8), it can be seen that the possibility of measuring the correct ground state energy is $1 - O(A^2t^2)$. After 2^D gates, where D is the number of binary digits that will be measured by PEA, the probability of state $\left|0\right\rangle \left|\psi\right\rangle_s$ should be still large enough. Set the final coefficient to be $1 - \frac{1}{8}$, then

$$(1 - O(A^2t^2))^{2^D} = 1 - \frac{1}{8} \tag{2.9}$$

$$2^{-D} = O(A^2t^2). \tag{2.10}$$

The error of the energy from the phase measurement is $\epsilon_1 = O(A^2t^2)$. The error of the energy from PEA is $\epsilon_2 = O(2^{-D}/t) = O(A^2t)$. Combining these errors together the total error becomes $\epsilon = O(\epsilon_1 + \epsilon_2) = O(A^2t)$.

For the second order Trotter-Suzuki decomposition

$$\mathrm{e}^{-\mathrm{i}Ht} - \prod_{\mathrm{i}=0}^{L} \mathrm{e}^{-\frac{\mathrm{i}\alpha_\mathrm{i} h_\mathrm{i} t}{2}} \prod_{\mathrm{i}=L}^{0} \mathrm{e}^{-\frac{\mathrm{i}\alpha_\mathrm{i} h_\mathrm{i} t}{2}} = O(A^3t^3), \tag{2.11}$$

a similar analysis can be done and the error will be $\epsilon = O(A^3t^2)$.

2.3.3 Complexity Analysis

n qubits are required for the state and at least 1 extra qubit is required for PEA process. In this way, the qubit complexity is $O(n)$.

If the precision of the ground state energy needs to be D bit, $O(2^D Ln)$ standard gates, i.e. single qubit gates and $CNOT$ gates, are required to implement the PEA. Since $L = O(n^4)$ for

molecular systems and $2^D = O(\frac{1}{A^2t^2}) = O(\frac{A^2}{\epsilon^2})$, the total gate complexity would be $O(\frac{n^5}{(\epsilon/A)^2})$ for Trotter-PEA method.

2.4 1^{st} order Direct-PEA Method

2.4.1 The Procedure of the Method

Apart from Trotter-Suzuki decomposition, there are still other methods to approximate propagator, such as Taylor series. It was proposed[28] that for any given H and large κ, an approximately unitary operator can be constructed by

$$U = I - \mathrm{i}\frac{H}{\kappa},\ \kappa \gg \sum_{\mathrm{i}=1}^{L} |\alpha_{\mathrm{i}}| \geq ||H||. \tag{2.12}$$

When $|\psi\rangle_s$ is an eigenstate of H and E the corresponding eigenenergy, we have

$$U|\psi\rangle_s = \left(I - \mathrm{i}\frac{H}{\kappa}\right)|\psi\rangle_s \approx \mathrm{e}^{-\mathrm{i}\frac{H}{\kappa}}|\psi\rangle_s = \mathrm{e}^{-\mathrm{i}\frac{E}{\kappa}}|\psi\rangle_s . \tag{2.13}$$

The eigenenergy E is encoded directly in the approximate phase and PEA may be used to extract it out. This is the motivation behind directly implementing the Hamiltonian in quantum simulation.

To implement the non-unitary matrix U, one way is to enlarge the state space and construct a unitary operator U_r[25] with similar properties. Rewrite U as

$$U = I - \frac{\mathrm{i}}{\kappa}\sum_{\mathrm{j}=1}^{L} \alpha_{\mathrm{j}} h_{\mathrm{j}} = \sum_{\mathrm{j}=0}^{L} \beta_{\mathrm{j}} V_{\mathrm{j}}, \tag{2.14}$$

in which $\beta_{\mathrm{j}} \geq 0$ and V_{j} is equal to $\mathrm{i}h_{\mathrm{j}}$ or $-\mathrm{i}h_{\mathrm{j}}$ based on β_{j}. By introducing a m-qubit ancilla register where $m = \lceil \log_2 L \rceil$, a multi-control gate, V, can be constructed to satisfy

$$V|\mathrm{j}\rangle_a |\psi\rangle_s = |\mathrm{j}\rangle_a V_{\mathrm{j}} |\psi\rangle_s . \tag{2.15}$$

Construct a unitary operator B that acts on ancilla qubits and has the property

$$B\left|0\right\rangle_a = \frac{1}{\sqrt{s}} \sum_{\mathrm{j}=0}^{2^m-1} \sqrt{\beta_{\mathrm{j}}} \left|\mathrm{j}\right\rangle_a, \ s = \sum_{\mathrm{j}=0}^{2^m-1} \beta_{\mathrm{j}}, \tag{2.16}$$

in which β_{j} are defined as 0 when $L < \mathrm{j} < 2^m$. Then U_r can be defined as

$$U_r = (B^\dagger \otimes I^{\otimes n}) V (B \otimes I^{\otimes n}). \tag{2.17}$$

Applying U_r on the input state $\left|0\right\rangle_a \left|\psi\right\rangle_s$ we obtain

$$\begin{aligned}
U_r \left|0\right\rangle_a \left|\psi\right\rangle_s &= (B^\dagger \otimes I^{\otimes n}) V (B \otimes I^{\otimes n}) \left|0\right\rangle_a \left|\psi\right\rangle_s \\
&= (B^\dagger \otimes I^{\otimes n}) V \frac{1}{\sqrt{s}} \sum_{\mathrm{j}=0}^{2^m} \sqrt{\beta_{\mathrm{j}}} \left|\mathrm{j}\right\rangle_a \left|\psi\right\rangle_s \\
&= (B^\dagger \otimes I^{\otimes n}) \frac{1}{\sqrt{s}} \sum_{\mathrm{j}=0}^{2^m} \sqrt{\beta_{\mathrm{j}}} \left|\mathrm{j}\right\rangle_a V_{\mathrm{j}} \left|\psi\right\rangle_s \\
&= \Pi (B^\dagger \otimes I^{\otimes n}) \frac{1}{\sqrt{s}} \sum_{\mathrm{j}=0}^{2^m} \sqrt{\beta_{\mathrm{j}}} \left|\mathrm{j}\right\rangle_a V_{\mathrm{j}} \left|\psi\right\rangle_s \\
&\quad + (I^{\otimes m+n} - \Pi)(B^\dagger \otimes I^{\otimes n}) \frac{1}{\sqrt{s}} \sum_{\mathrm{j}=0}^{2^m} \sqrt{\beta_{\mathrm{j}}} \left|\mathrm{j}\right\rangle_a V_{\mathrm{j}} \left|\psi\right\rangle_s \\
&= (B\left|0\right\rangle_a)^\dagger \frac{1}{\sqrt{s}} \sum_{\mathrm{j}=0}^{2^m} \sqrt{\beta_{\mathrm{j}}} \left|\mathrm{j}\right\rangle_a V_{\mathrm{j}} \left|\psi\right\rangle_s + \sum_{\mathrm{j}=1}^{\mathrm{j}=2^m} \left|\mathrm{j}\right\rangle_a \left|u_{\mathrm{j}}\right\rangle_s \\
&= \frac{1}{s} \left|0\right\rangle_a U \left|\psi\right\rangle_s + \left|\Phi_1^\perp\right\rangle .
\end{aligned} \tag{2.18}$$

Here $\Pi = \left|0\right\rangle_a \left\langle 0\right|_a \otimes I^{\otimes n}$ and $\left|\Phi_1^\perp\right\rangle$ is defined as a state orthogonal to $\left|0\right\rangle_a \left|\psi\right\rangle_s$. Then the non-unitary operator U can be implemented by applying the unitary operator U_r as seen in Figure 2.3

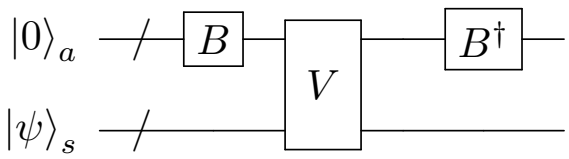

Figure 2.3. Gate U_r in Direct PEA circuit, gates V and B are shown in Eq. (2.15) and Eq. (2.16)

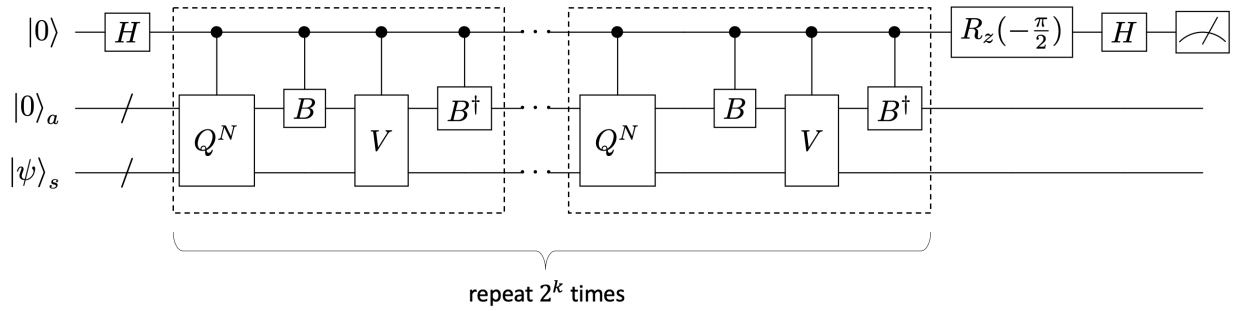

Figure 2.4. The quantum circuit for the Direct PEA method considering oblivious amplitude amplification.

Since $\kappa \gg ||H|| \geq E$, the eigenenergy for the state $|\psi\rangle_s$ is successfully implemented in the phase:

$$\begin{aligned} U_r |0\rangle_a |\psi\rangle_s &= \frac{1 - \mathrm{i}\frac{E}{\kappa}}{s} |0\rangle_a |\psi\rangle_s + |\Phi_1^\perp\rangle \\ &= \frac{\sqrt{1 + \frac{E^2}{\kappa^2}}}{s} \mathrm{e}^{-\mathrm{i}\tan^{-1}\frac{E}{\kappa}} |0\rangle_a |\psi\rangle_s + |\Phi_1^\perp\rangle \\ &= p\mathrm{e}^{-\mathrm{i}\tan^{-1}\frac{E}{\kappa}} |0\rangle_a |\psi\rangle_s + \sqrt{1-p^2} |\Phi^\perp\rangle , \end{aligned} \tag{2.19}$$

in which p is defined by $\frac{\sqrt{1+\frac{E^2}{\kappa^2}}}{s}$, and $|\Phi^\perp\rangle$ is normalized. This U_r gate can then be used for PEA or iterative PEA to solve the eigenenergy.

To make sure the output is accurate after PEA process, p is demanded to be as close to 1 as possible. Oblivious amplitude amplification[38] helps to amplify the probability without affecting phase in this case. Define the helper operator U_0 and the rotational operator Q as

$$U_0 = 2 |0\rangle_a \langle 0|_a - I^{\otimes m} \tag{2.20}$$

$$Q = U_r(U_0 \otimes I^{\otimes n})U_r^\dagger(U_0 \otimes I^{\otimes n}). \tag{2.21}$$

The probability of $|0\rangle_a |\psi\rangle_s$ can be increased by performing Q multiple times after U_r operator. The details are in the next Error Analysis section. The quantum circuit for the Direct-PEA that considers oblivious amplitude amplification is plotted in 2.4. The controlled U^{2^k} gate in the Figure 2.1 is replaced by the repeated dashed boxes in 2.4.

By using the same circuit and procedure as the Trotter-PEA, except replacing U by $U_q = Q^N U_r$, the ground state energy of water molecule can be obtained, as shown in Figure 2.5.

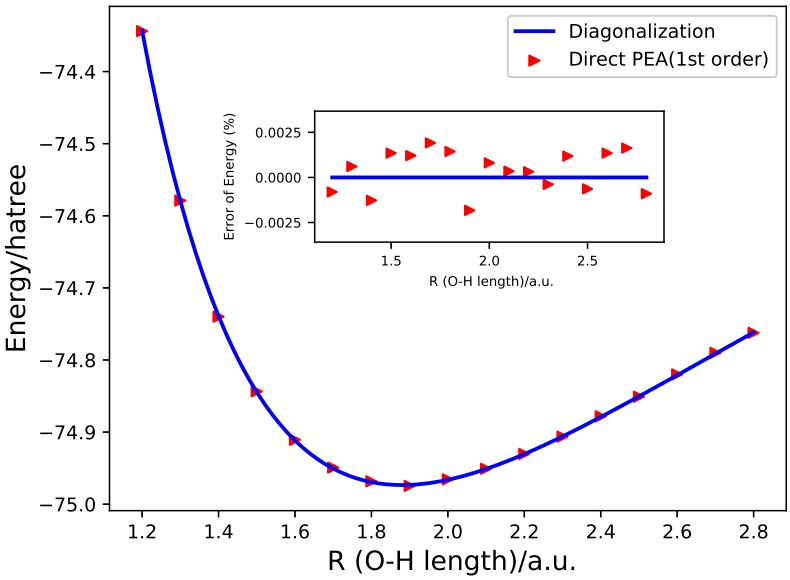

Figure 2.5. Ground State Energy Curve for H_2O, as a function of the bond length O-H in a.u. for 1^{st} order Direct-PEA. Errors are shown in the window of th figure.

2.4.2 Error Analysis

Eq. 2.19 can be rewritten as

$$U_r \left|0\right\rangle_a \left|\psi\right\rangle_s = \cos\theta e^{-i\tan^{-1}\frac{E}{\kappa}} \left|0\right\rangle_a \left|\psi\right\rangle_s + \sin\theta \left|\Phi^{\perp}\right\rangle, \tag{2.22}$$

in which $A = \sum_{i=1}^{2^m-1} \beta_i = \sum_{i=1}^{L} |\alpha_i| \geq |E|$, $\theta = \arccos \frac{\sqrt{1+\frac{E^2}{\kappa^2}}}{1+\frac{A}{\kappa}}$. By applying the operator Q N times after U_r, the resulting state becomes

$$\begin{aligned} Q^N U_r \left|0\right\rangle_a \left|\psi\right\rangle_s &= (-1)^N \cos((2N+1)\theta) e^{-i\tan^{-1}\frac{E}{\kappa}} \left|0\right\rangle_a \left|\psi\right\rangle_s + \sin((2N+1)\theta) \left|\Phi^{\perp}\right\rangle \\ &= p_f \left|0\right\rangle_a \left|\psi\right\rangle_s + \sqrt{1-p_f^2} \left|\Phi^{\perp}\right\rangle. \end{aligned} \tag{2.23}$$

The idea is, when κ is large, we have

$$\frac{\sqrt{1+\frac{E^2}{\kappa^2}}}{1+\frac{A}{\kappa}} \approx \frac{1}{1+\frac{A}{\kappa}}, \tag{2.24}$$

$$\theta = \cos^{-1}\frac{1}{1+\frac{A}{\kappa}} \approx \theta, \tag{2.25}$$

In this way, by choosing large N and κ to satisfy $(2N+1)\theta = \boldsymbol{\pi}$, which means $\frac{A}{\kappa} = \frac{1}{\cos(\frac{\pi}{2N+1})} - 1$, we are able to get $\cos((2N+1)\theta) \approx -1$. Since

$$\begin{aligned}\theta - \theta &= \cos^{-1}(\frac{\sqrt{1+\frac{E^2}{\kappa^2}}}{1+\frac{A}{\kappa}}) - \cos^{-1}(\frac{1}{1+\frac{A}{\kappa}}) \\ &= \frac{\sqrt{2}}{4}\eta^2(\frac{A}{\kappa})^{\frac{3}{2}} + O((\frac{A}{\kappa})^{\frac{5}{2}}),\end{aligned} \tag{2.26}$$

where $\eta = |\frac{E}{A}| \leq 1$, after N rotations we have

$$\begin{aligned}|p_f| &= |\cos((2N+1)\theta)| \\ &= \cos((2N+1)(\theta-\theta)) \\ &= 1 - \frac{(2N+1)^2}{16}\eta^4(\frac{A}{\kappa})^3 + O((\frac{A}{\kappa})^4) \\ &= 1 - \frac{\boldsymbol{\pi}^6}{2^{11}}\eta^4\frac{1}{N^4} + O(\frac{1}{N^5}).\end{aligned} \tag{2.27}$$

This means if N is large enough and we set

$$\kappa = \frac{A\cos(\frac{\pi}{2N+1})}{1-\cos(\frac{\pi}{2N+1})}, \tag{2.28}$$

we are able to amplify the probability of $|0\rangle_a |\psi\rangle_s$ to be extremely close to 1.

If D-digit accuracy are needed after the PEA step, we have to make sure that after 2^D gates of $U_q = Q^N U_r$, the probability of state $|0\rangle_a |\psi\rangle_s$ is still large. Assuming the threshold is $1 - \frac{1}{2^3}$, then the following formulas needs to be satisfied:

$$|p_f|^{2^D} = 1 - \frac{1}{2^3} \tag{2.29}$$

$$2^{-D} = \frac{\pi^6 \eta^4}{2^{11} \ln(\frac{8}{7})} \frac{1}{N^4} + O(\frac{1}{N^5}) \tag{2.30}$$

$$D = \min\{\log_2(\frac{2^{11} \ln(\frac{8}{7})}{\pi^6 \eta^4}) + 4 \log_2 N\} \approx -1.81 + 4 \log_2 N \tag{2.31}$$

Because the phase φ got from D-digit output are used used approximate $\frac{1}{2\pi} \tan^{-1} \frac{-E}{\kappa}$, and the error for the phase is 2^{-D}, the error of the energy is

$$\begin{aligned} \epsilon = \tan(2\pi * 2^{-D}) \times \kappa &= \frac{\pi^5 \eta^4}{2^7 \ln(\frac{8}{7})} \frac{1}{N^2} + O(\frac{1}{N^3}) \\ &\approx \frac{17.90 \eta^4 A}{N^2} \leq \frac{17.90}{N^2} A \end{aligned} \tag{2.32}$$

2.4.3 Complexity Analysis

n qubits are required for a molecular system's state and at least $m = \lceil \log_2(L) \rceil$ qubits are needed to represent the ancilla state. We also need at least 1 qubit for multi-control Toffoli gates in B gate construction[39], and at least 1 qubit for PEA process. Since $L = O(n^4)$, the qubit complexity is $O(n)$.

The construction of B operator can be done through Householder transformation

$$B = I - \frac{2}{\langle u|u\rangle_a} |u\rangle \langle u|_a , \tag{2.33}$$

where $|u\rangle_a = B|0\rangle_a - |0\rangle_a$. The complexity of this gate has been analyzed before[28], [40]–[42]. Since Givens rotation $G_{L-2,L-1}(\theta_{L-1})$ can nullify $B_{0,L-1}$, it can also nullify all $B_{\mathrm{j},L-1}$ for $\mathrm{j} \neq L-1$ and update $B_{L-1,L-1}$ to 1 due to B's special form. $G^T_{L-2,L-1}(\theta_{L-1})$ would nullify all $B_{L-1,\mathrm{j}}$ except $B_{L-1,L-1}$. For all indexes smaller than $L-1$ but larger than 1, we will do

the same thing. At the end we can choose $G_{1,1}(\theta_1)$ to update the last 4 elements of B and finally obtain an identity matrix. Thus we have:

$$G_{1,1}(\theta_1)\prod_{\mathrm{i}=2}^{L-1}G_{\mathrm{i}-1,\mathrm{i}}(\theta_{\mathrm{i}})B\prod_{\mathrm{i}=L-1}^{2}G^T_{\mathrm{i}-1,\mathrm{i}}(\theta_{\mathrm{i}})=I, \tag{2.34}$$

$$B=\prod_{\mathrm{i}=L-1}^{2}G^T_{\mathrm{i}-1,\mathrm{i}}(\theta_{\mathrm{i}})G^T_{1,1}(\theta_1)\prod_{\mathrm{i}=2}^{L-1}G_{\mathrm{i}-1,\mathrm{i}}(\theta_{\mathrm{i}}). \tag{2.35}$$

Under this construction, B operator can be represented as a product of $2L-3$ Givens rotation matrices. Since each Givens rotational matrix can be expressed by at most m m-control Toffoli gates, each of which costs $O(m^2)$ standard gates[8], [39], a total of $O(Lm^3)=O(L\log^3 n)$ gates are needed for B construction.

For *select*(V) gate, we need $O((n+m)L)$ standard gates. In this case, U_r requires $O(L\log^3 n+(n+m)L)=O(n^5)$ gates. Since U_0 only needs $O(m)$ standard gates, Q also requires $O(n^5)$ standard gates, which leads the gate complexity of U_q to be $O(Nn^5)$. Since from Eq. 2.32, $N=O(\frac{1}{(\epsilon/A)^{\frac{1}{2}}})$, PEA for D digit accuracy would result in a total complexity of $O(2^DNn^5)=O(\frac{n^5}{(\epsilon/A)^{2.5}})$ standard gates.

2.5 2^{nd} order Direct-PEA Method

2.5.1 The Procedure of the Method

The propagator $\mathrm{e}^{-\mathrm{i}Ht}$ can also be expanded up to the second order Taylor series[29]:

$$U=I-\mathrm{i}Ht-\frac{H^2t^2}{2}=\mathrm{e}^{-\mathrm{i}Ht}+O((At)^3), \tag{2.36}$$

which would be a good approximation when $O(At)$ is very small. Since U is non-unitary, we have to construct a unitary operator U_{r2} to implement it into the quantum circuit. Define operators B_2 and P as

$$B_2\left|00\right\rangle=\frac{\sqrt{t}\left|00\right\rangle+\left|01\right\rangle+\frac{t}{\sqrt{2}}\left|10\right\rangle}{\sqrt{1+t+\frac{t^2}{2}}}, \tag{2.37}$$

$$P = \begin{bmatrix} I^{\otimes n} & 0 & 0 & 0 \\ 0 & 0 & I^{\otimes m} & 0 \\ 0 & I^{\otimes m} & 0 & 0 \\ 0 & 0 & 0 & I^{\otimes n} \end{bmatrix}. \tag{2.38}$$

With the help of U_r defined in 1^{st} order Direct-PEA, we can construct U_{r2} as shown in Figure 2.6.

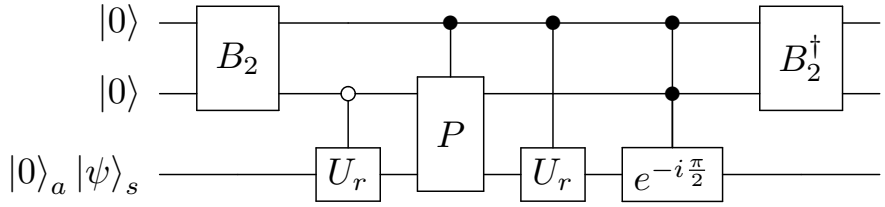

Figure 2.6. Gate U_{r2} in 2^{nd} order Direct-PEA circuit, with B_2 and P defined in Eq. (2.37) and Eq. (2.38)

Applying U_{r2} to the initial state, we will get

$$\begin{aligned} U_{r2} |00\rangle |0\rangle_a |\psi\rangle_s &= \frac{1 - \mathrm{i}\frac{Et}{A} - \frac{E^2t^2}{2A^2}}{1 + t + \frac{t^2}{2}} |00\rangle |0\rangle_a |\psi\rangle_s + \sum_{\mathrm{j}=1}^{2^{m+2}} |\mathrm{j}\rangle |v_\mathrm{j}\rangle_s \\ &= \frac{\sqrt{1 + \frac{E^4t^4}{4A^2}}}{1 + t + \frac{t^2}{2}} \mathrm{e}^{-\mathrm{i}\tan^{-1}\frac{\frac{Et}{A}}{1+\frac{E^2t^2}{2A}}} |00\rangle |0\rangle_a |\psi\rangle_s + |\Psi_1^\perp\rangle, \end{aligned} \tag{2.39}$$

in which $A = \sum_{\mathrm{i}=1}^{2^m-1} \beta_\mathrm{i} = \sum_{\mathrm{i}=1}^{L} |\alpha_\mathrm{i}| \geq |E|$ and $|\Psi_1^\perp\rangle$ is perpendicular to $|00\rangle |0\rangle_a |\psi\rangle_s$. The coefficient of state $|00\rangle |0\rangle_a |\psi\rangle_s$ can be increased using oblivious amplitude amplification just as in the previous section. Then we can perform PEA or iterative PEA to get the phase, $-\tan^{-1}\frac{\frac{Et}{A}}{1+\frac{E^2t^2}{2A}}$, which gives the ground state energy corresponding to the ground state $|\psi\rangle_s$, as shown in Figure 2.7.

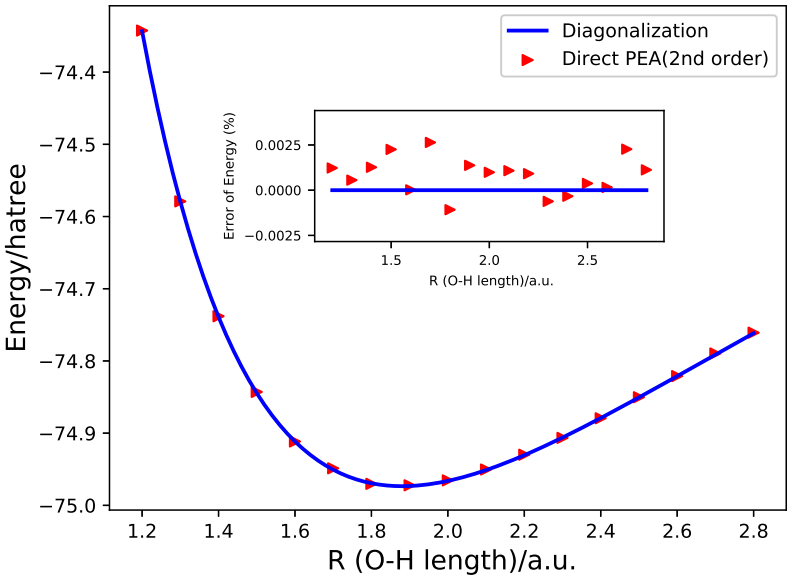

Figure 2.7. Ground State Energy Curve for H_2O, as a function of the bond length O-H in a.u. for 2^{st} order Direct-PEA. Errors are shown in the window of each figure.

2.5.2 Error Analysis

The output state in Eq. (2.39) can be rewritten as

$$\begin{aligned} U_{r2}\left|00\right\rangle\left|0\right\rangle_a\left|\psi\right\rangle_s &= \frac{\sqrt{1+\frac{E^4t^4}{4A^2}}}{1+t+\frac{t^2}{2}} \mathrm{e}^{-\mathrm{i}\tan^{-1}\frac{\frac{Et}{A}}{1+\frac{E^2t^2}{2A}}}\left|00\right\rangle\left|0\right\rangle_a\left|\psi\right\rangle_s + \left|\Psi_1^{\perp}\right\rangle \\ &= p\mathrm{e}^{-\mathrm{i}\tan^{-1}\frac{\frac{Et}{A}}{1+\frac{E^2t^2}{2A}}}\left|00\right\rangle\left|0\right\rangle_a\left|\psi\right\rangle_s + \sqrt{1-p^2}\left|\Psi^{\perp}\right\rangle \\ &= \cos\theta\mathrm{e}^{-\mathrm{i}\tan^{-1}\frac{\frac{Et}{A}}{1+\frac{E^2t^2}{2A}}}\left|00\right\rangle\left|0\right\rangle_a\left|\psi\right\rangle_s + \sin\theta\left|\Psi^{\perp}\right\rangle, \end{aligned} \tag{2.40}$$

in which $A = \sum_{\mathrm{i}=1}^{2^m-1} \beta_{\mathrm{i}} = \sum_{\mathrm{i}=1}^{L} |\alpha_{\mathrm{i}}| \geq |E|, \theta = \cos^{-1} \frac{\sqrt{1+\frac{E^4t^4}{4A^2}}}{1+t+\frac{t^2}{2}}$. Applying $Q_2 = U_{2r}(U_0^+ \otimes I^{\otimes n})U_{2r}^\dagger(U_0^+ \otimes I^{\otimes n})$, where $U_0^+ = 2|00\rangle|0\rangle_a\langle 0|_a\langle 00| - I^{\otimes m+2}$, to do oblivious amplitude amplification, we can get

$$\begin{aligned} Q_2^N U_{2r}|00\rangle|0\rangle_a|\psi\rangle_s &= (-1)^N \cos((2N+1)\theta) \mathrm{e}^{-\mathrm{i}\tan^{-1}\frac{\frac{Et}{A}}{1+\frac{E^2t^2}{2A}}}|0\rangle_a|\psi\rangle_s \\ &\quad + \sin((2N+1)\theta)|\Psi^\perp\rangle_{a+s+2} \\ &= p_f|00\rangle|0\rangle_a|\psi\rangle_s + \sqrt{1-p_f^2}|\Psi^\perp\rangle_{a+s+2} \end{aligned} \tag{2.41}$$

Let $\theta = \cos^{-1}\frac{1}{1+t+\frac{t^2}{2}}$ and choose large N and small t to satisfy $(2N+1)\theta = \boldsymbol{\pi}$, then

$$t = -1 + \sqrt{\frac{2}{\cos\frac{\pi}{2N+1}} - 1} = \frac{\boldsymbol{\pi}^2}{8N^2} + O(\frac{1}{N^3}), \tag{2.42}$$

and we can get the difference between θ and θ

$$\theta - \theta = \cos^{-1}\frac{\sqrt{1+\frac{E^4t^4}{4A^2}}}{1+t+\frac{t^2}{2}} - \cos^{-1}\frac{1}{1+t+\frac{t^2}{2}} = \frac{\sqrt{2}}{16}\eta^4 t^{\frac{7}{2}} + O(t^{\frac{9}{2}}), \tag{2.43}$$

in wihch $\eta = |\frac{E}{A}| \leq 1$. After N rotations, we have

$$\begin{aligned} |p_f| &= |\cos((2N+1)\theta)| \\ &= \cos((2N+1)(\theta-\theta)) \\ &= 1 - \frac{(2N+1)^2}{16^2}\eta^8 t^7 + O(t^8) \\ &= 1 - \frac{\boldsymbol{\pi}^{14}}{2^{27}}\eta^8\frac{1}{N^{12}} + O(\frac{1}{N^{13}}) \end{aligned} \tag{2.44}$$

This means if we set N large enough, and set $t = -1 + \sqrt{\frac{2}{\cos\frac{\pi}{2N+1}} - 1}$, we can amplify the probability of $|00\rangle|0\rangle_a|\psi\rangle_s$ to be as close to 1 as we want.

Now we are taking $U_{q2} = Q_2^N U_{r2}$ to encode the energy into the phase. If we would like D-digit accuracy, we have to make sure that after 2^D gates of U_{q2}, the probability of state

$|0\rangle_a |\psi\rangle_s$ is still large. By setting the final coefficient as $1 - \frac{1}{2^3}$, the following formula should be satisfied:

$$|p_f|^{2^D} = 1 - \frac{1}{2^3} \tag{2.45}$$

$$2^{-D} = \frac{\boldsymbol{\pi}^{14}\eta^8}{2^{27}\ln(\frac{8}{7})}\frac{1}{N^{12}} + O(\frac{1}{N^{13}}) \tag{2.46}$$

$$D = \min\{\log_2(\frac{2^{27}\ln(\frac{8}{7})}{\boldsymbol{\pi}^{14}\eta^8}) + 12\log_2 N\} \approx 0.974 + 12\log_2 N \tag{2.47}$$

Since D-digit output from PEA gives us the phase φ to approximate $-\frac{1}{2\boldsymbol{\pi}}\tan^{-1}\frac{\frac{Et}{A}}{1+\frac{E^2t^2}{2A}}$ and the error of phase is 2^{-D}, we get the error of the energy E to be:

$$\epsilon = \frac{\boldsymbol{\pi}^{13}\eta^8}{2^{23}\ln\frac{8}{7}}\frac{A}{N^{10}} + O(\frac{A}{N^{11}}) \approx \frac{2.59\eta^8 A}{N^{10}} \leq \frac{2.59}{N^{10}}A \tag{2.48}$$

We can see that by taking large N and set corresponding small t, we are able to control the accuracy of PEA process.

2.5.3 Complexity Analysis

We need n qubits to represent the system state, $m = \lceil\log_2(L)\rceil + 2$ qubits to represent the ancilla state. So the qubit complexity is still $O(n)$ for the 2^{nd} order Direct-PEA.

When constructing U_{r2}, gate U_r takes $O(n^5)$ standard gates, gate P takes $O(L) = O(n^4)$ standard gates, B_2, $B_2^\dagger$ and phase gate $\mathrm{e}^{-\mathrm{i}\frac{\pi}{2}}$ only takes a small constant of standard gates. So the gate complexity of U_{r2} is still $O(n^5)$. Then Q_2 also requires $O(n^5)$ standard gates because U_0^+ just needs O(m) standard gates. Since $N = O(\frac{1}{(\epsilon/A)^{0.1}})$, PEA for D digit accuracy would result in a total of $O(2^D N n^5) = O(\frac{n^5}{(\epsilon/A)^{1.3}})$ standard gates.

2.6 Direct Measurement Method

2.6.1 The Procedure of the Method

Another way to calculate the ground state energy is by direct measurement after implementing a given Hamiltonian in quantum circuit. Since Direct-PEA (1^{st} order) method has

already introduced a way to implement non-unitary matrix U into circuit, Hamiltonian implementation is straightforward. We can just replace U in method B by $U = H = \sum_{\mathrm{j}=1}^{L} \alpha_{\mathrm{j}} h_{\mathrm{j}}$, and obtain U_r such that:

$$\begin{aligned} U_r \left|0\right\rangle_a \left|\psi\right\rangle_s &= \frac{1}{s} \left|0\right\rangle_a U_r \left|\psi\right\rangle_s + \left|\Phi_1^{\perp}\right\rangle \\ &= \frac{E}{A} \left|0\right\rangle_a \left|\psi\right\rangle_s + \left|\Phi_1^{\perp}\right\rangle . \end{aligned} \tag{2.49}$$

By measuring ancilla qubits multiple times, we can get the energy of the ground state $\left|\psi\right\rangle_s$ through multiplying A by the square root of probability that the ancillary register state is $\left|0\right\rangle_a$. The ground state energy of water molecule calculated by this method is in Figure 2.8.

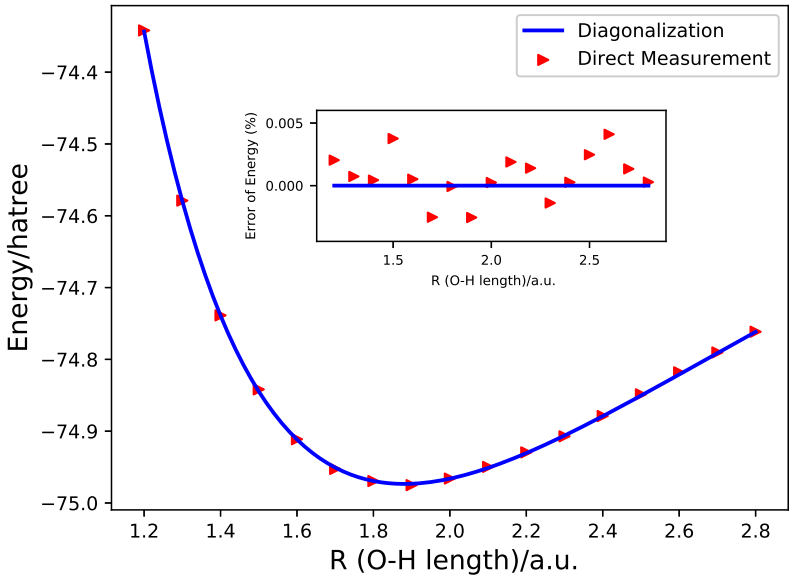

Figure 2.8. Ground State Energy Curve for H_2O, as a function of the bond length O-H in a.u. for 2^{st} order Direct-PEA. Errors are shown in the window of the figure.

This method can also be used for non-Hermitian Hamiltonians. If now the eigenvalue for $|\psi\rangle_s$ is a complex number $E = |E|e^{i\theta}$, by replacing U by $U = H$ in method B, we would have:

$$U_r |0\rangle_a |\psi\rangle_s = \frac{|E|e^{i\theta}}{A} |0\rangle_a |\psi\rangle_s + |\Phi_1^{\perp}\rangle , \tag{2.50}$$

and can obtain $|E|$ through measurements. Then by replacing U by for example $U = I + H$ in method B, we would be able to determine the phase of the complex eigenenergy.

2.6.2 Error Analysis

After applying the gate U_r:

$$U_r |0\rangle_a |\psi\rangle_s = \frac{E}{A} |0\rangle_0 |\psi\rangle_s + |\Phi_1^{\perp}\rangle \tag{2.51}$$

We obtain the eigenenergy of state $|\psi\rangle_s$ by calculating probability of the wanted state: $|0\rangle_a |\psi\rangle_s$. The standard error of E by X measurements is:

$$\sigma = \frac{|E|}{\sqrt{X}} \sqrt{1 - \frac{E^2}{A^2}} \tag{2.52}$$

2.6.3 Complexity Analysis

The number of required qubits for Direct Measurement Method is the sum of system and ancilla qubits: O(n). Since only one U_r gate is enough, the complexity of the standard gates is $O(n^5)$. Since now the result of measurements is a binomial distribution, to measure the Energy E to accuracy(standard deviation) ϵ, we have to make $X = O(\frac{E^2}{\epsilon^2})$ measurements.

2.7 Variational Quantum Eigensolver(VQE) Method

2.7.1 The Procedure of the Method

The variational quantum eigensolver method has been put forward by Aspuru-Guzik and coworkers to calculate the ground state energies[30]–[33], which is a hybrid method

of classical and quantum computation. According to this method, an adjustable quantum circuit is constructed at first to generate a state of the system. This state is then used to calculate the corresponding energy under the system's Hamiltonian. Then by a classical optimization algorithm, like Nelder-Mead method, parameters in circuit can be adjusted and the generated state will be updated. Finally, the minimal energy will be obtained. The detailed circuit for the quantum part of our algorithm is shown in Figure 2.9. To make the expression more clear, we represent parameters in vector form, as follows: $\boldsymbol{\theta} = (\boldsymbol{\theta_1}, \boldsymbol{\theta_2}..., \boldsymbol{\theta_D})$, $\boldsymbol{\theta}_\mathrm{i} = (\boldsymbol{\theta}_{\mathrm{i},\mathbf{0}}, \boldsymbol{\theta}_{\mathrm{i},\mathbf{1}}..., \boldsymbol{\theta}_{\mathrm{i},\mathbf{11}})$, $\boldsymbol{\theta}_{\mathrm{i,j}} = (\theta_{\mathrm{i,j},1}, \theta_{\mathrm{i,j},2}, \theta_{\mathrm{i,j},3},)$, $\boldsymbol{\varphi} = (\boldsymbol{\varphi_1}, \boldsymbol{\varphi_2}..., \boldsymbol{\varphi_n})$, $\boldsymbol{\varphi_k} = (\varphi_{k,1}, \varphi_{k,2}, \varphi_{k,3})$.

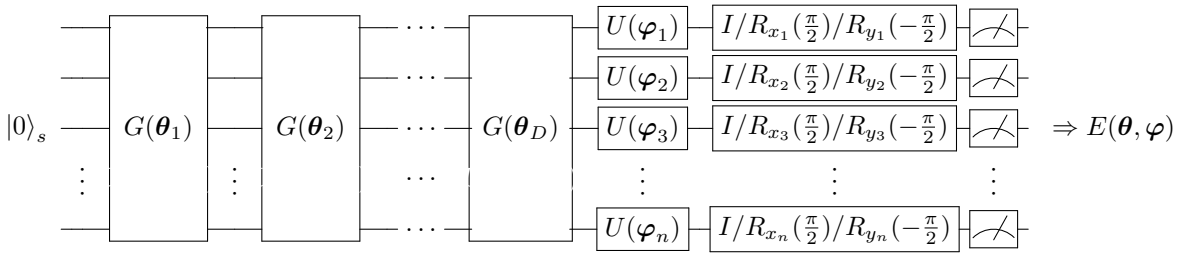

Figure 2.9. Circuit for state preparation and corresponding energy evaluation. $G(\boldsymbol{\theta}_\mathrm{i})$ is entangling gate, here we are taking the gate like Figure 2.10. $U(\boldsymbol{\varphi}_k)$ is an arbitrary single-qubit rotation and is equal to $R_z(\varphi_{k,1})R_x(\varphi_{k,2})R_z(\theta_{k,3})$ with parameters $\varphi_{k,1}$,$\varphi_{k,2}$ and $\varphi_{k,3}$ that can be manipulated. By increasing the number of layers, d, of our circuit, we are able to produce more complex states.

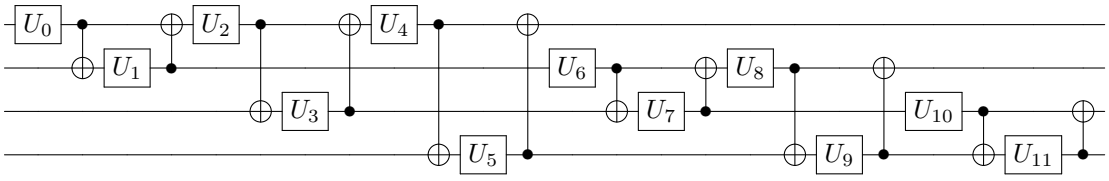

Figure 2.10. Example entangling circuit $G(\boldsymbol{\theta}_\mathrm{i})$ for 4-qubit system. There are 12 arbitrary single-qubit gates U_j, a simplified written way for $U(\boldsymbol{\theta}_{\mathrm{i,j}})$, which is $R_z(\theta_{\mathrm{i,j},1})R_x(\theta_{\mathrm{i,j},2})R_z(\theta_{\mathrm{i,j},3})$ with parameters $\theta_{\mathrm{i,j},1}$,$\theta_{\mathrm{i,j},2}$ and $\theta_{\mathrm{i,j},3}$ that can be manipulated. Each 2 qubits are entangled sequentially. Entangling gate $G(\boldsymbol{\theta}_\mathrm{i})$ for n-qubit system is similar to this gate, but then it has $n(n-1)$ arbitrary single-qubit gates and $\boldsymbol{\theta}_\mathrm{i}$ has $3n(n-1)$ parameters.

We are using d layers of gate $G(\boldsymbol{\theta}_\mathrm{i})$ in Figure 2.9 to entangle all qubits together. Here we introduce a hardware-efficient $G(\boldsymbol{\theta}_\mathrm{i})$, and we call this method Pairwise VQE. The example

gate of $G(\boldsymbol{\theta}_{\mathrm{i}})$ for 4 qubits is shown in Figure 2.10. The entangling gate for 6-qubit system H_2O is similar: every 2 qubits are modified by single-qubit gates and entangled by $CNOT$ gates. By selecting initial value of all $\boldsymbol{\theta}_{\mathrm{i}}$ and $\boldsymbol{\varphi}_k$, system state can be prepared by d layers $G(\boldsymbol{\theta}_{\mathrm{i}})$ gates and arbitrary single gates $U(\boldsymbol{\varphi}_{\mathrm{j}})$. Then average value of each term in Hamiltonian H, $\langle h_{\mathrm{j}}\rangle$, can be evaluated by measuring qubits many times after going through gates like I or $R_{x_{\mathrm{j}}}(\frac{\pi}{2})$ or $R_{y_{\mathrm{j}}}(-\frac{\pi}{2})$. For example, if $h_{\mathrm{j}} = I_0X_1Y_2Z_3$, then

$$\begin{aligned}
\langle h_{\mathrm{j}}\rangle &= \langle I_0X_1Y_2Z_3\rangle_\psi = \langle\psi|\, I_0X_1Y_2Z_3\,|\psi\rangle \\
&= (\langle\psi|\, R_{y_1}(\frac{\pi}{2})R_{x_2}(-\frac{\pi}{2}))I_0(R_{y_1}(-\frac{\pi}{2})X_1R_{y_1}(\frac{\pi}{2})) \\
&\quad (R_{x_2}(\frac{\pi}{2})Y_2R_{x_2}(-\frac{\pi}{2}))Z_3(R_{y_1}(-\frac{\pi}{2})R_{x_2}(\frac{\pi}{2})\,|\psi\rangle) \\
&= \langle I_0Z_1Z_2Z_3\rangle_\psi \quad \text{, where } |\psi\rangle = R_{y_1}(-\frac{\pi}{2})R_{x_2}(\frac{\pi}{2})\,|\psi\rangle\,,
\end{aligned} \tag{2.53}$$

So we can let the quantum state $|\psi\rangle$ go through gates $R_{y_1}(-\frac{\pi}{2})$ and $R_{x_2}(\frac{\pi}{2})$ and then measure the result state multiple times to get $\langle h_{\mathrm{j}}\rangle$. The energy corresponding to the state can be obtained by $\langle H\rangle(\boldsymbol{\theta},\boldsymbol{\varphi}) = \sum_{\mathrm{j}=1}^{L}\alpha_{\mathrm{j}}\langle h_{\mathrm{j}}\rangle(\boldsymbol{\theta},\boldsymbol{\varphi})$. Then $\boldsymbol{\theta}$ and $\boldsymbol{\varphi}$ can be updated by classical optimization method and $\langle H\rangle(\boldsymbol{\theta},\boldsymbol{\varphi})$ can reach the minimal step by step. An example of convergence process for H_2O's ground state energy is shown in Figure 2.11. The ground state energy curve calculated by this method is shown in Figure 2.12. One thing needs to mention is that the error peak in the middle can not be reduced after we tried different classical optimizers. A possible reason is that there is a local minimal around the ground state of H_2O at that configuration and traps our optimizers.

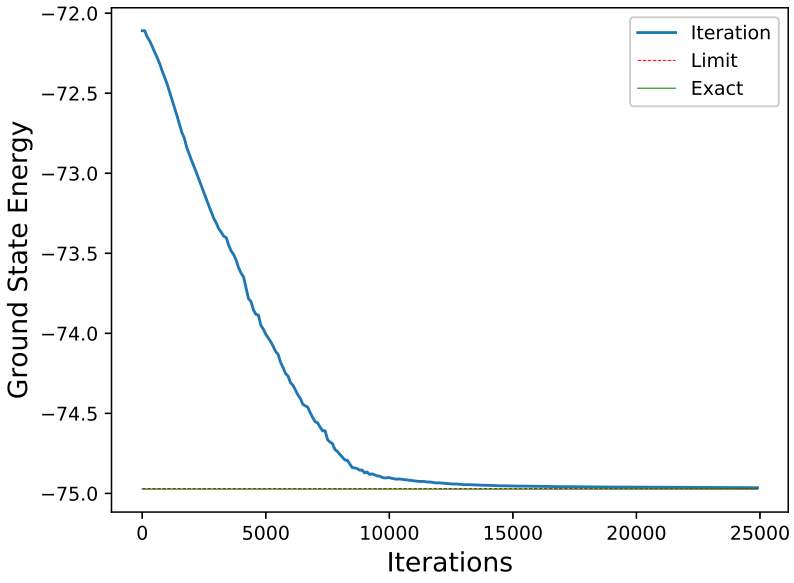

Figure 2.11. Convergence of ground state energy of H_2O for fixed O-H bond length = 1.9 a.u., as number of iterations increases. The lines for exact ground state energy and for the limit almost overlap.

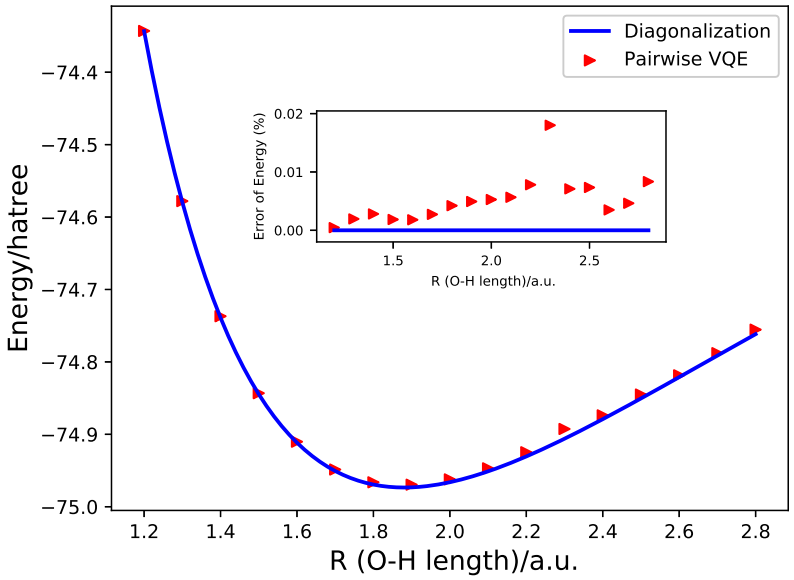

Figure 2.12. Ground state energy curve for H_2O, as a function of O-H bond length in a.u. for Pairwise VQE. Errors are shown in the window of the figure. We take $|0\rangle_s$ as initial input, $d = 1$ layer and use Nelder-Mead algorithm for optimization.

2.7.2 Error and Complexity Analysis

The number of qubits required for Pairwise VQE is n, and the gate complexity is $O(n^2 d)$, where d is the number of entangling gate layers. Assume we made X_i measurements for calculating $\langle h_\mathrm{i} \rangle$, its accuracy(standard deviation) would be $\epsilon_\mathrm{i} = \frac{1}{X_\mathrm{i}}$. With $X = \sum_{\mathrm{i}=1}^{L} X_\mathrm{i}$ measurements, the accuracy of Hamiltonian would be

$$\epsilon = \sum_{\mathrm{i}=1}^{L} \frac{a_\mathrm{i}}{\sqrt{X_\mathrm{i}}} \leq \sqrt{\sum_{\mathrm{i}=1}^{L} a_\mathrm{i}^2} \sqrt{\sum_{\mathrm{i}=1}^{L} \frac{1}{X_\mathrm{i}}} \leq A \sqrt{\sum_{\mathrm{i}=1}^{L} \frac{1}{X_\mathrm{i}}} \tag{2.54}$$

If $X_\mathrm{i} = \frac{X}{L}$, we have $\epsilon \leq \frac{AL}{\sqrt{X}}$, then we need $X = \frac{A^2 L^2}{\epsilon^2} = \frac{A^2 n^8}{\epsilon^2}$ measurements to achieve accuracy ϵ. Considering the number of iterations for optimization, N_{iter}, the total number of measurements is $\frac{A^2 n^8}{\epsilon^2} N_{iter}$.

2.8 Comparison of Methods

The Hamiltonian of the water molecule is calculated for O-H bond lengths ranging from 0.5 a.u. to 2.9 a.u., using the above introduced methods. This Hamiltonian is used in all five of the methods discussed within this chapter. For the first four methods, the input state of system is the ground state of the H_2O molecule. For each of the four methods, the resulting ground state energy curve can be calculated to arbitrary accuracy. The results from each method is compared with result from a direct diagonalization of the Hamiltonian, as shown in each graph. From Figure 2.2-2.8, it can be seen that all of these methods are effective in obtaining the ground state energy curve of the water molecule. Pairwise VQE is also used to obtain the ground state energy curve. The energy convergence process when O-H bond length equals 1.9 a.u. is shown in Figure 2.11. The ground state energy curve calculated by this method is shown in Figure 2.12. In this simulation, d is selected to be 1, and $G(\boldsymbol{\theta}_\mathrm{i})$ is constructed as described above, and it can already give a pretty good result. This shows Pairwise VQE a very promising method for solving electronic structure problems. Furthermore, Pairwise VQE has only $O(n^2 d)$ gate complexity and doesn't require initial input of the ground state, which makes it more practical for near-term applications on a quantum computer.

Qubit requirement, gate complexity and number of measurements of different methods are shown in TABLE 2.1. When counting gate complexities, we decompose all gates into single qubit gates and CNOT gates. While Pairwise VQE needs exactly n qubits, the other methods require extra number of qubits. In terms of gate scaling, Pairwise VQE also needs the least gates, which enables it to better suit the applications on near and intermediate term quantum computers. Among the remaining four methods, Direct Measurement requires less number of gates than the others. PEA-type methods have an advantage that they can give an accurate result under only $O(1)$ measurements. However, they need more qubits compared with the previous two methods and demands many more gates if smaller error is required. Due to huge gate complexity, these PEA-type algorithms would be put into practice only when the decoherence problem has been better solved. Among these three PEA based methods, in terms of the gate complexity, Direct-PEA(2^{nd} order) requires less number of gates than the traditional Trotter-PEA and Direct-PEA(1^{st} order). One more thing to mention is that here the second quantization form Hamiltonian is based on STO-3G, so there are $O(n^4)$ terms. If a more recent dual form of plane wave basis [43] is used, the number of terms can be reduced to $O(n^2)$, and the asymptotic scaling in TABLE 2.1 would also be reduced. To be specific, for PEA-type methods, upper bounds of gate complexities would be proportional to n^3 rather than n^5, and Number of Measurements for Pairwise VQE would be proportional to n^4 rather than n^8. As can be seen, these reductions wouldn't influence the comparison made above.

Table 2.1. Complexity of different methods. n is the number of qubits for molecular system, 6 for water. $A = \sum_{i=1}^{L} |\alpha_i|$ can serve as the scale of energy. E is the exact value of ground energy. ϵ is the accuracy of energy we want to reach. d is the number of layers we used in Pairwise VQE. N_{iter} is the number of iterations for optimization in Pairwise VQE.

Method	#Qubits	Gate Complexity	#Measurements
Trotter-PEA	$O(n)$	$O(\frac{n^5}{(\epsilon/A)^2})$	$O(1)$
Direct-PEA(1^{st} order)	$O(n)$	$O(\frac{n^5}{(\epsilon/A)^{2.5}})$	$O(1)$
Direct-PEA(2^{nd} order)	$O(n)$	$O(\frac{n^5}{(\epsilon/A)^{1.3}})$	$O(1)$
Direct Measurement	$O(n)$	$O(n^5)$	$O(\frac{E^2}{\epsilon^2})$
Pairwise VQE	$O(n)$	$O(n^2 d)$	$O(\frac{A^2 n^8}{\epsilon^2} N_{iter})$

2.9 Excited States

All the mentioned 5 methods can also be used for the excited state energy calculation. PEA-type methods and Direct Measurement method can be directly used by replacing the input ground state by an excited state. The complexity for the calculation would stay the same. The energy accuracy for excited states are similar to that for the ground state. For VQE, a publication [44], [45] recently presents a quantum subspace expansion algorithm (QSE) that calculates excited state energies. They approximate a "subspace" of low-energy excited states from linear combinations of states of the form $O_i |\psi\rangle_s$, where $|\psi\rangle_s$ is the ground state determined by VQE and O_i are chosen physically motivated quantum operators. By diagonalizing the matrix with elements $\langle\psi|_s O_i^\dagger H O_j |\psi\rangle_s$ calculated by VQE, one is able to find the energies of excited states.

Figure 2.13 shows the simulation of the first six excited states' energy curves of the water molecule from our 6-qubit Hamiltonian, calculated by PEA-type methods and Direct Measurement method. It can be seen that the 5^{th} excited energy curve indicates a shape resonance phenomenon, which can be described by a non-Hermitian Hamiltonian with complex eigenvalues. The life time of the resonance state is associated with the imaginary part of the eigenvalues. In this way, to solve the resonance problem, we can seek to solve the eigenvalues of non-Hermitian Hamiltonians.

Some work has been done on this track to solve the resonance problem by quantum computers. By designing a general quantum circuit for non-unitary matrices, Daskin et al.[46] explored the resonance states of a model non-Hermitian Hamiltonian. To be specific, he introduced a systematic way to estimate the complex eigenvalues of a general matrix using the standard iterative phase estimation algorithm with a programmable circuit design. The bit values of the phase qubit determines the phase of eigenvalue, and the statistics of outcomes of the measurements on the phase qubit determines the absolute value of the eigenvalue. Other approaches for solving complex eigenvalues can also be applied for this resonance problem. For example, Wang et al. [47] proposed a measurement-based quantum algorithms for finding eigenvalues of non-unitary matrices. Terashima et al.[48] introduced a universal nonunitary quantum circuit by using a specific type of one-qubit non-unitary gates, the controlled-NOT gate, and all one-qubit unitary gates, which is also useful for finding the eigenvalues of a non-hermitian Hamiltonian matrix. More about resonances will be included in the next chapter.

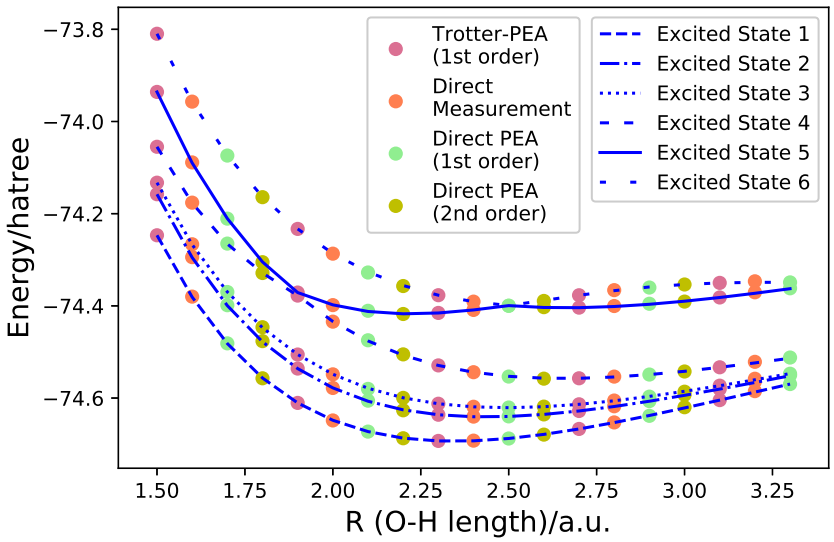

Figure 2.13. Excited states' energy curves for H_2O, as a function of the bond length O-H in a.u.. Markers with different colors represent data points calculated from different methods. Only a few points for each method are drawn for illustration. Energy curves in different line styles are calculated from exact diagonalization of Hamiltonian matrix.

2.10 Conclusion

In this chapter, several recently proposed quantum algorithms are compared when they are used to compute the electronic state energies of the water molecule. These methods include Trotter-PEA method based on the first order Trotter-Suzuki decomposition, 1^{st} and 2^{rd} order Direct-PEA methods based on direct implementation of the truncated propagator, Direct Measurement method based on direct implementation of the Hamiltonian and Pairwise PEA method, a VQE algorithm with a designed ansatz.

After deriving the Hamiltonian of the water molecule using the STO-3G basis set, the research explains in detail how each method works and gives their qubit requirements, gate complexities and measurement scaling. It also calculates the ground state energy curves for the water molecule using all five methods. All methods are able to provide an accurate result. By comparing these methods, it is concluded that the 2^{nd} order Direct-PEA provides the most efficient circuit implementations in terms of gate complexity. With large scale quantum computation, the 2^{nd} order direct method seems to better suit large molecule systems. In addition, since Pairwise VQE requires the least qubit number, it is the most practical method for near-term applications on the current available quantum computers.

Moreover, the PEA-type methods and Direct Measurement method are used to solve excited state energy curves for the water molecule. The fifth excited state energy curve implies shape resonance.

3. THE DESIGN AND IMPLEMENTATION OF THE FULLY CONTROLLED VQE

3.1 Introduction

As introduced in the last chapter, VQE is the most practical way to search for the ground state and the ground state energy of a molecular system in near-term quantum computers. The most important question for VQE is how to design an efficient quantum circuit to produce an ansatz state that approximates the ground state well. Recently researchers are trying to construct different parameterized quantum circuits[33], [49], [50] for VQE for systems like LiH or H_2O. Generally, by applying designed circuit $Gate(\vec{\theta})$ to the input state $|\psi_{input}\rangle$, we have output state

$$|\psi_{output}\rangle = Gate(\vec{\theta})\,|\psi_{input}\rangle\,. \tag{3.1}$$

The parameters $\vec{\theta}$ are set to some initial values at first. They will be updated by classical optimization methods, such as Nelder-Mead, to find an output state with minimal energy.

It is hard to directly search the ground state of Hamiltonian in the whole space. Say our system needs n qubits, then we need to search all states in the n-qubit space to obtain the ground state finally. That would take us at least $2^n - 1$ parameters to control $Gate(\vec{\theta})$ and thus the 2^n-d output state $|\psi_{output}\rangle$, which makes the algorithm intractable. A common way is to use fewer parameters than needed to approximate the ground state. By taking many layers of basic parameterized entangling gates, we can assume the circuit is complicated enough to approach the ground state. Although this design is practical and has even been applied in real quantum computers[33], it is hard to tell the real representability of the circuit. Most of the time, people have to try different entangling circuit designs and find the one that works best for the problem. Worse still, the best circuit design for one system may not be good for another system.

Here we propose a quantum circuit design, which we call Fully Controlled VQE (FCVQE), that can reduce gate complexity for ansatz state preparation and also has clear representability. For a system with n orbitals and m electrons, the design is able to explore all possible

state configurations with a cost of $O(\binom{n}{m})$ gates. The gate complexity can be further reduced to $O(poly(n))$ if we only consider limited electron number excitation, such as single, double, triple, and quadruple excitation.

3.2 General Design of the Fully Controlled VQE

Assume that a system with n orbitals and m electrons is in interest, and we would like to find the system's ground state energy. After the standard procedure of Jordan-Wigner transformation, each orbital would be mapped to a qubit, while qubit state $|1\rangle$ means the orbital is occupied and $|0\rangle$ means unoccupied. Since only $\binom{n}{m}$ basis states represent m-electron states, the space of possible ground state can be reduced from a 2^n-d real sphere to a $\binom{n}{m}$-d one. In the following part, we will use a sequence of Givens Rotation matrices to create an ansatz state that can fully explore m-electron states.

Take $|k_1\rangle$ as Hartree-Fock state $|\psi_{HF}\rangle$, where k_1 represents the decimal number for the binary form qubit state. We mark the indices of $\binom{n}{m}$ m-electron states out of 2^n electron states to be a set: $\{k_1, k_2, k_3..., k_{\binom{n}{m}}\}$, and assign a set of parameters $\{\theta_2, \theta_3..., \theta_{\binom{n}{m}}\}$ to each index except k_1. Every parameter θ_i would be used to construct a Givens Rotation matrix as follows:

$$
G_\mathrm{i}(\theta_\mathrm{i}) = \begin{array}{c} \\ 0 \\ \vdots \\ k_1 \\ \vdots \\ k_\mathrm{i} \\ \vdots \\ k_{\binom{n}{m}} \\ \vdots \end{array}
\begin{array}{c}
\begin{array}{ccccccccc} 0 & \dots & k_1 & \dots & k_\mathrm{i} & \dots & k_{\binom{n}{m}} & \dots & \end{array} \\
\begin{bmatrix}
1 & & & & & & & & \\
& \ddots & & & & & & & \\
& & \cos\theta_\mathrm{i} & & -\sin\theta_\mathrm{i} & & & & \\
& & & \ddots & & & & & \\
& & \sin\theta_\mathrm{i} & & \cos\theta_\mathrm{i} & & & & \\
& & & & & \ddots & & & \\
& & & & & & 1 & & \\
& & & & & & & \ddots &
\end{bmatrix}
\end{array}, \tag{3.2}
$$

where the diagonal and off-diagonal elements not shown in Eq. 3.2 are 1 and 0 respectively. Each Givens Rotation matrix can be constructed by $O(n)$ $(n-1)$-control quantum gates. The details of construction and complexity analysis will be illustrated in next section.

By applying a sequence of Givens Rotation matrix, $Gate(\vec{\theta}) = \prod_{\mathrm{i}=2}^{\binom{n}{m}} G_{\mathrm{i}}(\theta_{\mathrm{i}})$, to the input Hartree-Fock state, $|\psi_{HF}\rangle = |k_1\rangle$, the output state would be

$$|\psi_{output}\rangle = Gate(\vec{\theta})\,|\psi_{HF}\rangle = \prod_{\mathrm{j}=2}^{\binom{n}{m}} \cos\theta_{\mathrm{j}}\,|k_1\rangle + \sum_{\mathrm{i}=2}^{\binom{n}{m}} \sin\theta_{\mathrm{i}} \prod_{\mathrm{j}=\mathrm{i}+1}^{\binom{n}{m}} \cos\theta_{\mathrm{j}}\,|k_{\mathrm{i}}\rangle \tag{3.3}$$

$$= \begin{array}{c} \vdots \\ k_1 \\ \vdots \\ k_2 \\ \vdots \\ k_3 \\ \vdots \\ k_{\mathrm{i}} \\ \vdots \\ k_{\binom{n}{m}} \\ \vdots \end{array} \begin{bmatrix} \vdots \\ \prod_{\mathrm{j}=2}^{\binom{n}{m}} \cos\theta_{\mathrm{j}} \\ \vdots \\ \sin\theta_2 \prod_{\mathrm{j}=3}^{\binom{n}{m}} \cos\theta_{\mathrm{j}} \\ \vdots \\ \sin\theta_3 \prod_{\mathrm{j}=4}^{\binom{n}{m}} \cos\theta_{\mathrm{j}} \\ \vdots \\ \sin\theta_{\mathrm{i}} \prod_{\mathrm{j}=\mathrm{i}+1}^{\binom{n}{m}} \cos\theta_{\mathrm{j}} \\ \vdots \\ \sin\theta_{\binom{n}{m}} \\ \vdots \end{bmatrix} \tag{3.4}$$

All elements in the right state of Eq. 3.4 are 0 except those indexed $\{k_1, k_2, ...k_{\binom{n}{m}}\}$. This state formula can represent any m-electron state that can be represented by real numbers, which means the ground state of Hamiltonian H can be represented by this state with properly selected parameters $\vec{\theta}$.

Using this $Gate(\vec{\theta})$ to produce ansatz state, we can then follow the standard procedure of VQE in the previous chapter and update $\vec{\theta}$ to find the ground state and the ground state energy of molecular systems. One thing worth to note is that, although it's guaranteed that some $\vec{\theta}$ can represent the ground state, the state may be trapped in a local minimum position during the optimization process.

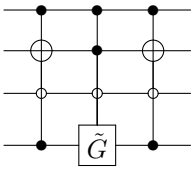

Figure 3.1. Quantum circuit for $G_{\mathrm{i}}(\theta_{\mathrm{i}})$ in a 4-qubit system, while $k_1 = 12$ and $k_{\mathrm{i}} = 9$.

3.3 Circuit Design for Givens Rotation Matrix

To construct the circuit for Givens Rotation matrix, $G_{\mathrm{i}}(\theta_{\mathrm{i}})$, we can use multi-controlled *NOT* gates and multi-controlled rotation gates. The intuition is to swap the basis states such that the rotation can be done in one qubit, then swap the basis states back. Say $G_{\mathrm{i}}(\theta_{\mathrm{i}})$ is applied on two basis states $|k_1\rangle$ and $|k_{\mathrm{i}}\rangle$, we can first pick up these two states with multi-controlled states. By flipping digits in $|k_1\rangle$ to make it only one qubit state different from $|k_{\mathrm{i}}\rangle$, we can rotate this qubit instead. Finally, after flipping states back, we successfully implement $G_{\mathrm{i}}(\theta_{\mathrm{i}})$ on the circuit.

Take a 4-qubit system for example and assume that we want to construct $G_{\mathrm{i}}(\theta_{\mathrm{i}})$ with $|k_1\rangle = |12\rangle = |1100\rangle$ and $|9\rangle = |1001\rangle$. FIG. 3.1 gives one of the ways to construct Givens Rotation Operator. Here in the figure the single qubit rotational gate $\tilde{G}$ is

$$\tilde{G} = \begin{bmatrix} \cos\theta_{\mathrm{i}} & -\sin\theta_{\mathrm{i}} \\ \sin\theta_{\mathrm{i}} & \cos\theta_{\mathrm{i}} \end{bmatrix}. \tag{3.5}$$

Before multi-controlled $\tilde{G}$, this circuit converts $|1001\rangle$ to $|1101\rangle$. Then the multi-control $\tilde{G}$ gate does rotation on $|1100\rangle$ and $|1101\rangle$. After that the circuit converts $|1101\rangle$ back to $|1001\rangle$.

For general cases, since each multi-control gate requires $O(n)$ standard gates[8], [39] and the whole circuit takes $O(n)$ multi-control gates, the total gate complexity for each Givens rotation matrix is $O(n^2)$.

For there are in total $O(\binom{n}{m})$ Givens Rotation matrices, the gate complexity of ansatz preparation circuit is $O(n^2\binom{n}{m})$. When m is small compared with orbital number n, or m is close to n, this circuit will take approximately $O(poly(n))$ gates for construction. However, if m is close to half of n, gate complexity can be exponential. To overcome this issue, we can

consider only the main components of the system's ground state, like the Hartree-Fock state, single excited state and double excited state. This step will reduce the gate complexity to polynomial.

3.4 Ground State Energy Curve of H_2 by IBM Qiskit Simulator

Here we apply the fully controlled VQE to solve the ground state energy of H_2. The Hamiltonian can be transformed into 4-qubit Pauli matrix form if we use STO-3G basis functions. Since there are only 6 possible 2-electron states, we need to apply 5 Givens Rotation matrix to the input Hatree-Fock state for ansatz state preparation. The state preparation circuit is as shown in Fig. 3.2.

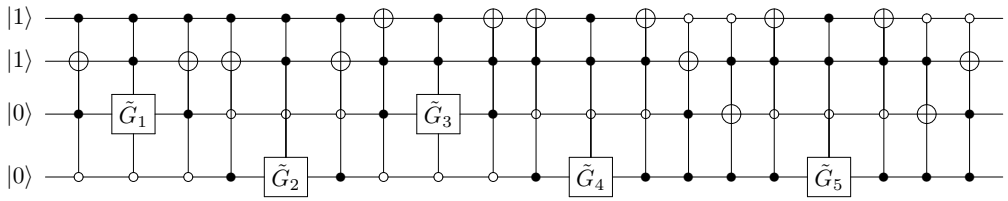

Figure 3.2. The fully controlled quantum circuit design for state preparation for H_2. $\tilde{G}_i$ is a gate which has a matrix format like Eq.3.5.

The circuit can be further simplified if we take system's symmetry into account: half spins are up and half are down. The updated circuit is as shown in Fig. 3.3.

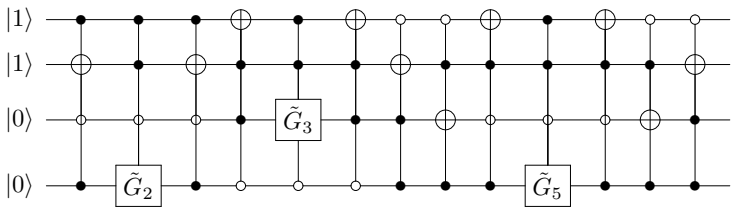

Figure 3.3. The simplified circuit for state preparation for H_2.

IBM has developed a platform called Qiskit[51], by which people can run quantum algorithms on both the simulators and the real quantum computers. Since the real quantum computer is still very noisy, we will use the simulator to verify our design. Multi-control

gates with more than three control qubits are not included in the Qiskit built-in gate library; thus, we need to decompose them into built-in gates. One of the easiest ways is to introduce ancilla qubits in the middle and decompose the circuit into Toffoli gates, two-qubit control gates, and single-qubit gates. After some classical optimization process, the ground state energy curve of H_2 is shown in Fig. 3.4. It can be seen that the error is negligible.

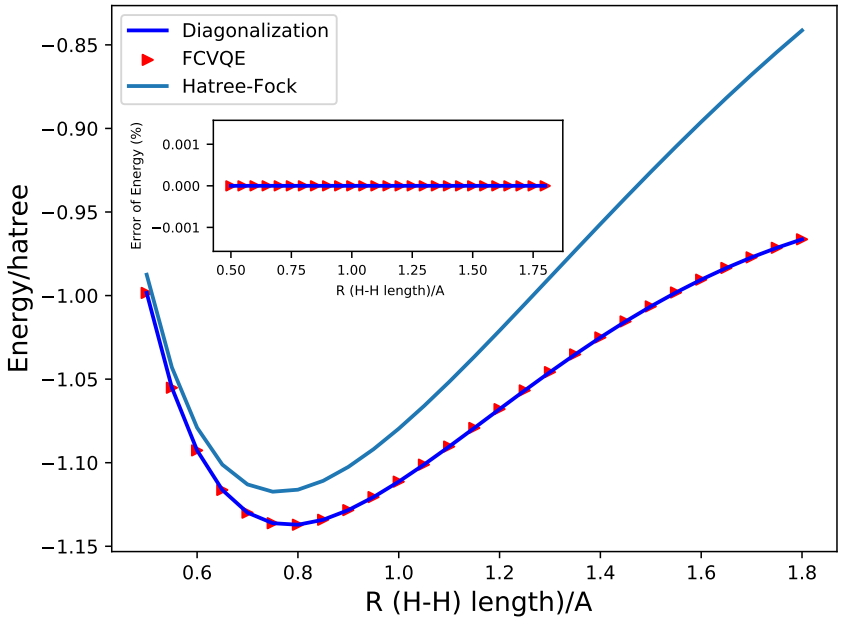

Figure 3.4. Ground state energy curve for H_2 under fully controlled VQE(FCVQE), as a function of bond length H-H in angstrom, calculated by IBM's simulator. Errors are shown in the window of the figure.

3.5 Ground State Energy Curves of Molecules by Self-designed Simulator

For larger systems, we can also get pretty accurate ground state energy curves using FCVQE. In terms of computational cost, fully controlled VQE in this section is carried out by a self-designed simulator using matrix manipulation.

One example is NaH. We use the STO-3G basis set and assume the 10 innermost orbitals are occupied. Then there are 2 electrons left in the outer 10 orbitals. Considering all possible 2-electron states, we have the ground state energy curve as Fig. 3.5 using FCVQE. It can be seen that almost all data points are perfect except for the divergent point in the

diagonalized curve. The reason may be that the state in the divergent points is complicated, and the classical optimization process falls into a local minimum.

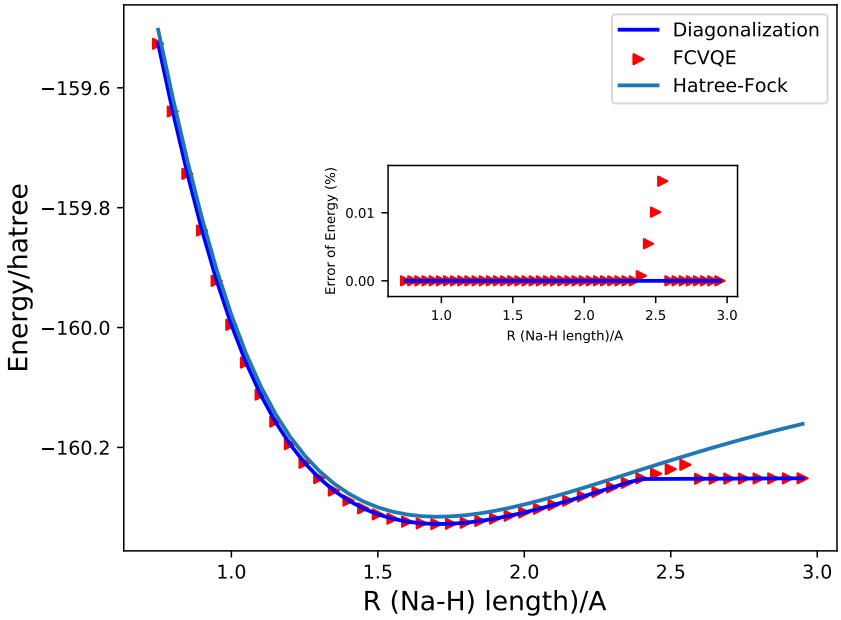

Figure 3.5. Ground state energy curve for NaH under fully controlled VQE, as a function of bond length Na-H in Å. Errors are shown in the window of the figure.

For H_2O, we also use the STO-3G basis set to do second quantization. Assuming that the 2 innermost orbitals are always occupied, we can transform the Hamiltonian to 12-qubit Pauli matrix form. To simplify the problem, we also assume the number of spin-up electrons is the same as spin-down electrons. Results corresponding to different excitation types are shown in Fig. 3.6. It can be seen that as more excited states are taken into account, the FCVQE gives a more accurate ground state energy curve.

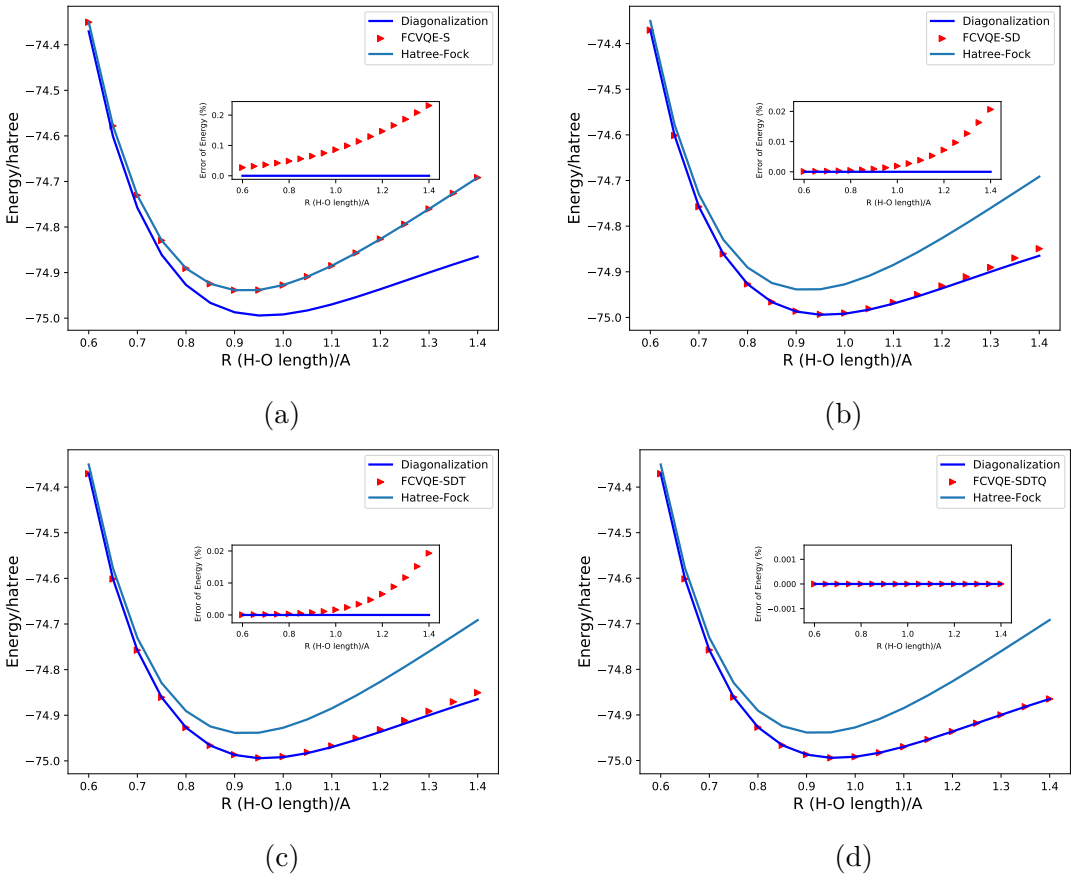

Figure 3.6. Ground State Energy Curve for H_2O as a function of the bond length O-H in Å. The red triangles are obtained by FCVQE that (a) considers only single excitation, (b) considers both single and double excitation, (c) considers single, double and triple excitation (d) considers single, double, triple, and quadruple excitation, and are compared with the Hartree-Fock ground state energy and the exact diagonalization. Errors are shown in the window of each figure.

The same procedure can be applied on N_2, except that we now assume the 8 innermost orbitals are always occupied. The ground state energy curves for N_2 are shown in Fig. 3.7. The ground state energy curve obtained by FCVQE gets closer to the diagonalized exact curve when more excitation are considered.

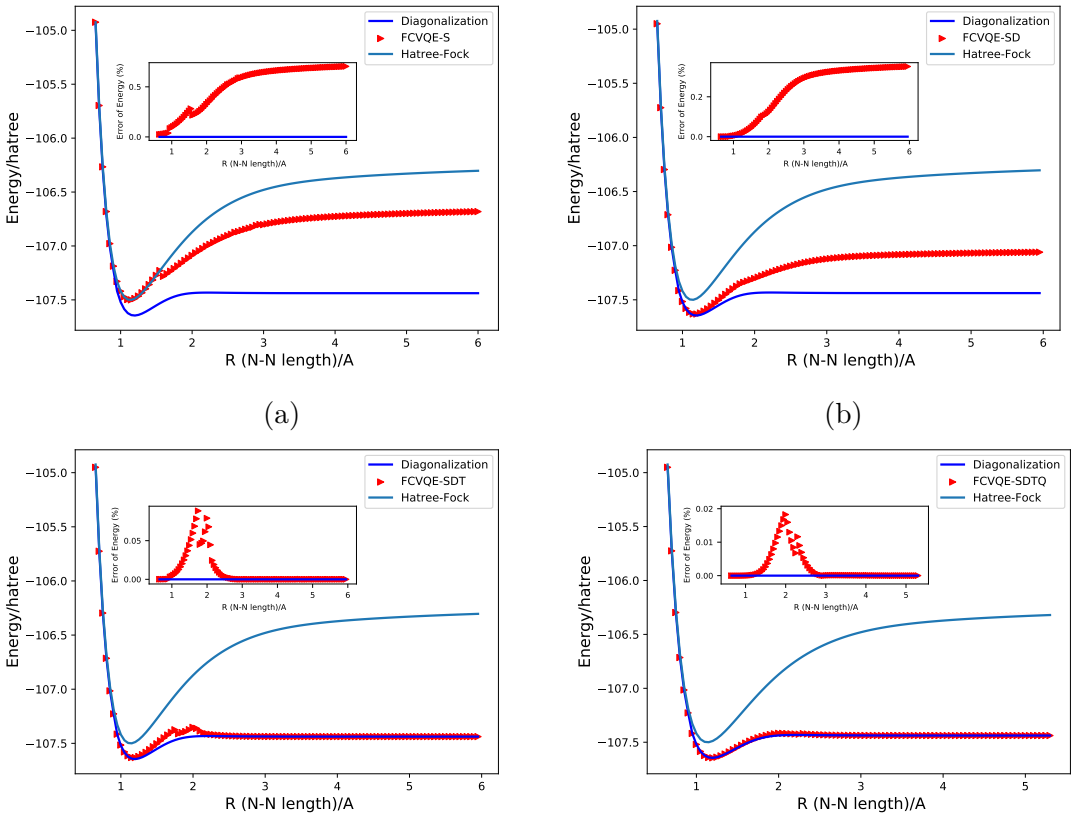

Figure 3.7. Ground State Energy Curve for N_2 as a function of the bond length N-N in Å. The red triangles are obtained by FCVQE that (a) considers only single excitation, (b) considers both single and double excitation, (c) considers single, double and triple excitation (d) considers single, double, triple, and quadruple excitation, and are compared with the Hartree-Fock ground state energy and the exact diagonalization. Errors are shown in the window of each figure.

If we consider all 6-electron states for N_2, the curve would be more accurate, as shown in Fig. 3.8.

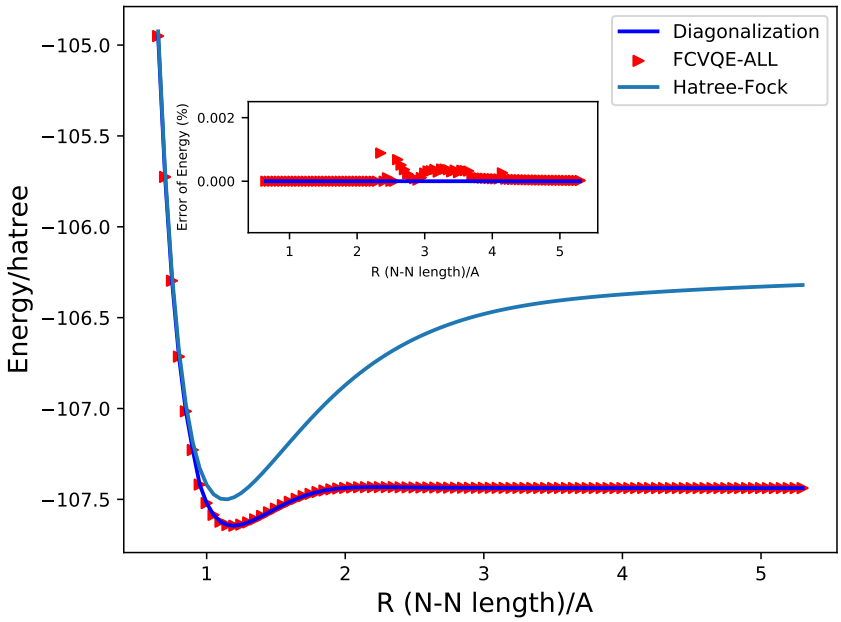

Figure 3.8. Ground State Energy Curve for N_2 as a function of the bond length N-N in Å using FCVQE. All 6-electron states are considered. Errors are shown in the window of each figure.

3.6 Complexity Analysis

For a system with n orbitals and m electrons, the qubit requirement for FCVQE is $O(n)$, including qubits to represent system state and ancilla qubits to decompose multi-controlled gates. Gate complexity for FCVQE depends on the number of Givens Rotation Operators, which is $O(\binom{n}{m})$, and the number of basic gates (one-qubit and two-qubit gates) for each Givens Rotation operator. In general, we need $O(n)$ n-controlled gates to do rotations between two basis states and need $O(n)$ basic gates for each n-controlled gate, so the gate complexity is $O(n^2)$. However, since we know the number of electrons is restricted to m during state preparation, only a constant number of n-controlled gates are required for Givens Rotation operators' construction. Thus the total complexity would be $O(n\binom{n}{m})$.

The number of Givens Rotation Operators in the above sequence can be intractable when $m \approx \frac{n}{2}$. However, it can be reduced if we consider some restrictions on the ground state wavefunction. For example, if the total number of electrons is even and half of them are assumed to be spin up, then only $\binom{n/2}{m/2}^2$ rather than $\binom{n}{m}$ states needs to be considered

in ansatz state preparation. Assuming that the ground state wavefunction contains only Hartree-Fock state and small-number electron excitation states from the Hartree-Fock state, the required number of Givens Rotation operators can be even lower. If up to k-electron excitation from $|\psi_{HF}\rangle$ are considered, the total complexity is $O(n\binom{n-k}{k}\binom{mk}{k})$. When k = 2, the total complexity becomes $O(n\binom{n-m}{2}\binom{m}{2}) \approx O(m^2n^3)$.

3.7 Summary and discussion

This chapter presents a new quantum circuit design for ansatz state preparation in VQE algorithm called FCVQE. A sequence of parameterized Givens Rotation matrices, which can be implemented with a polynomial number of standard single-qubit and two-qubit gates, will be applied to the input state to get the output state. Unlike other circuit designs that assume the output state has the representability to approximate the ground state of a given system, this design gives an explicit mathematical form for the output state with parameters and shows that this form will explore all possible states with proper parameter values.

The output state with initial parameters will then be used to evaluate the corresponding energy under the molecule's Hamiltonian of Pauli matrix form. Following standard VQE procedure, parameters will be updated to find the state with minimum energy. The energy would be approximate ground state energy, and as a byproduct, the final output state will be the ground state of this molecule system.

One thing needed to notify is that the VQE algorithm is essentially an optimization method. It can not avoid the local minimum problem, especially when the molecular system's size is large, and the Hamiltonian is complicated. This answers why some converged data points are still away from the exact result in the previous curves. One method for improvement is to use a better optimization method to jump out of the local minimum. An easier way is to try different initial values and take the minimum of those different experiments.

4. QUANTUM COMPUTING FOR ATOMIC AND MOLECULAR RESONANCES

4.1 Introduction

Resonance phenomena is common in nature since they exist in a wide range of fields, such as atomic and molecular physics, chemistry, molecular biology and technology. It is associated with intermediate or quasi-stationary states when a system breaks into multiple subsystems. For example, the phenomena appears when an excited atom autoionizes, an excited molecule disassociates unimolecularly, or a molecule attracts an electron and then the ion disassociates into stable ionic and neutral subsystems[52], [53].

We are not able to directly solve resonances from the Hamiltonians discussed in the last chapters. The reason is all those conventional Hamiltonians are Hermitian. By directly solving Hermitian Hamiltonians, we will get real eigenvalues and corresponding eigenfunctions in the L^2 Hilbert space that vanish at infinity. However, the decaying resonance states don't hold the boundary condition of vanishing at infinity, which means they can not be fully described by the scope of functions in L^2. Actually, they are associated with the Hamiltonians' complex eigenvalues. If we imposes outgoing boundary conditions on a Hamiltonians' eigenfunction, the corresponding complex eigenvalue, $E_{res} = E - \mathrm{i}\frac{\Gamma}{2}$, will reveal to us its resonance energy E and resonance width Γ. The reason why a Hermitian Hamiltonian has complex eigenvalues is that the non-Hermitian properties of an operator depends on both the operator itself and the functions it applies to. [52]

Then how can we obtain the complex eigenvalues of the Hamiltonian? One method proposed decades ago is called the complex rotation method, developed by [54]–[59]. We refer the readers to the book on non-Hermitian quantum mechanics by Moiseyev for more details and applications of the method [52]. Given a system Hamiltonian $H(\mathbf{r})$, where $\mathbf{r}$ represents electrons' coordinates, this method rotates $\mathbf{r}$ into the complex plane by θ, $\mathbf{r} \to \mathbf{r}\mathrm{e}^{\mathrm{i}\theta}$, and thus the Hamiltonian becomes a non-Hermitian $H(\mathbf{r}\mathrm{e}^{\mathrm{i}\theta})$. The system's resonance state's

energy E and width $\Gamma = \frac{1}{\tau}$, where τ is life time, can then be obtained by directly solving the corresponding complex eigenvalue of $H(\mathbf{r}e^{i\theta})$ operator,

$$E_\theta = E - \frac{i}{2}\Gamma. \tag{4.1}$$

The best resonance estimate is when the θ pauses or slows down in its trajectory [60]. This complex rotation method became prevalent at that time because it looks simple, and it can take use of conventional programs for eigenvalue calculation in molecular problems. Moreover, dimensional scaling and large order dimensional perturbation theory has been applied for complex eigenvalues using the complex rotation method [61], [62].

However, usually, a large basis set is necessary to predict resonances with good accuracy. For example, the Helium ^1S resonance uses 32 Hylleraas type functions for basis construction [63], the H_2^- $^2\Sigma_u^+(\sigma_g^2\sigma_u)$ resonance takes a total of 38 constructed Gaussian atomic basis [64]. They only pick a small set of electronic configurations for classical variational methods to calculate complex eigenvalues. The computational overhead will become overwhelming if more configurations, or more basis functions need to be considered, like when we want to have better accuracy, or when we simulate larger molecule systems. A promising way to overcome the escalation in computational resources is solving the problem by quantum computing methods in quantum computers.

As seen above, the resonance problem can be reduced to a problem of solving complex eigenvalues of a non-Hermitian Hamiltonian. Unfortunately, most quantum algorithms for the Hermitian Hamiltonian problem in our previous chapters can not be directly adapted to resonance calculation, because the complex-rotated, or complex-scaled Hamiltonian's non-Hermitian property. For example, for the conventional phase estimation algorithm (PEA), the propagator $e^{-iH(\mathbf{r}e^{i\theta})t}$ with trotterization [18] will be non-unitary and it can not be implemented in quantum circuit directly. In this way, a quantum algorithm for resonance calculation that can deal with non-Hermitian Hamiltonian is in need. Daskin et. al [46] proposed a circuit design that can solve complex eigenvalues of a general non-unitary matrix. The method applies the matrix rows to an input state one by one and estimate complex eigenvalues via a novel iterative PEA process. However, for molecular Hamiltonians, the

gate complexity of this general design is exponential in system size. In our previous publication[34], we briefly mentioned that our Direct Measurement method could be used to solve complex eigenvalues of non-Hermitian Hamiltonians with polynomial gates. This study, will extend the Direct Measurement method and apply it to simple molecular systems to obtain resonance properties. In particular, we will use IBM's Qiskit simulators and their real quantum computers to calculate these resonances.

4.2 Complex Scaled Hamiltonian

In this section, we present the steps needed to convert the complex-rotated Hamiltonian to a suitable form that can be simulated on a quantum computer. In the Born-Oppenheimer approximation, the electronic Hamiltonian of a molecular system can be written as a sum of electronic kinetic energy and potential energy of the form,

$$\begin{aligned} H &= T(\mathbf{r}) + V(\mathbf{r}), \\ T(\mathbf{r}) &= \sum_{\mathrm{i}} -\frac{1}{2}\nabla_{\mathrm{i}}^2, \\ V(\mathbf{r}) &= \sum_{\mathrm{i}} \sum_{\mathrm{j}>\mathrm{i}} \frac{1}{|\mathbf{r_i} - \mathbf{r_j}|} + \sum_{\mathrm{i},\sigma} \frac{Z_\sigma}{|\mathbf{r}_{\mathrm{i}} - \mathbf{R}_\sigma|}, \end{aligned} \tag{4.2}$$

where Z_σ is the σ_{th} nucleus' charge, $\mathbf{R}_\sigma$ is the σ_{th} nucleus' position, and $\mathbf{r}_{\mathrm{i}}$, $\mathbf{r}_{\mathrm{j}}$ represents the i_{th}, j_{th} electron's position. Now, the complex scaling method is applied to the study of molecular resonances within the framework of Born-Oppenheimer approximation. Following Moiseyev and coworkers[52] the electronic coordinates are dilated independently of the nuclear coordinates. After a complex rotation by θ, each electron's position $\mathbf{r}$ becomes $\mathbf{r}/\eta$, where $\eta = \mathrm{e}^{-\mathrm{i}\theta}$ and thus the new Hamiltonian becomes

$$H_\theta = T(\mathbf{r}/\eta) + V(\mathbf{r}/\eta), \tag{4.3}$$

$$T(\mathbf{r}/\eta) = \eta^2 \sum_{\mathrm{i}} -\frac{1}{2}\nabla_{\mathrm{i}}^2, \tag{4.4}$$

$$V(\mathbf{r}/\eta) = \eta \sum_{\mathrm{i}} \sum_{\mathrm{j}>\mathrm{i}} \frac{1}{|\mathbf{r}_{\mathrm{i}} - \mathbf{r}_{\mathrm{j}}|} + \eta \sum_{\mathrm{i},\sigma} \frac{Z_\sigma}{|\mathbf{r}_{\mathrm{i}} - \eta\mathbf{R}_\sigma|}. \tag{4.5}$$

The eigenstates of H_θ include resonance states, whose corresponding complex eigenvalues reveal resonance states' energies and lifetimes [55], [65], as stated in Eq.(4.1). A scaling parameter α is commonly used in the complex rotation process to better locate resonances, which makes $\eta = \alpha e^{-i\theta}$.

After choosing a proper orthogonal basis set $\{\psi_i(\mathbf{r})\}$, the Hamiltonian can be converted into a second quantization form,

$$H_\theta = \sum_{i,j} h_{ij} a_i^\dagger a_j + \frac{1}{2} \sum_{i,j,k,l} h_{ijkl} a_i^\dagger a_j^\dagger a_k a_l, \tag{4.6}$$

where $a_i^\dagger$ and a_i are fermionic creation and annihilation operators, and coefficients h_{ij}, h_{ijkl} can be calculated by

$$\begin{aligned} h_{ij} &= \int \psi_i^*(\mathbf{r})(-\eta^2 \frac{1}{2}\nabla_i^2 + \eta \sum_\sigma \frac{Z_\sigma}{|\mathbf{r} - \eta \mathbf{R}_\sigma|})\psi_j(\mathbf{r}), \\ h_{ijkl} &= \int \psi_i^*(\mathbf{r_1})\psi_j^*(\mathbf{r_2}) \frac{\eta}{|\mathbf{r}_1 - \mathbf{r}_2|} \psi_k(\mathbf{r_2})\psi_l(\mathbf{r_1}). \end{aligned} \tag{4.7}$$

With Jordan-Wigner transformation[11],

$$\begin{aligned} a_j^\dagger &= \frac{1}{2}(X_j - iY_j) \otimes Z_{j-1}^{\rightarrow}, \\ a_j &= \frac{1}{2}(X_j + iY_j) \otimes Z_{j-1}^{\rightarrow}, \end{aligned} \tag{4.8}$$

in which X, Y and Z are the Pauli X, Y and Z operators, and

$$Z_{j-1}^{\rightarrow} = Z_{j-1} \otimes Z_{j-2} \otimes Z_0, \tag{4.9}$$

the Hamiltonian will be further transformed into Pauli operators as

$$H_\theta = \sum_{i=0}^{L-1} c_i P_i. \tag{4.10}$$

In the summation, c_i represents a complex coefficient, and P_i represents an up to n-local tensor product of Pauli operators, where n is the size of the basis set. Alternatively, Bravyi-

Kitaev transformation or parity transformation can also be used in the final step to obtain the Hamiltonian in the qubit space[11].

The above process is the same as the conventional Hamiltonian derivation in quantum computing for electronic structure calculations of bound states. Here for resonance calculations, to make the Hamiltonian convenient to use in the Direct Measurement method, we rewrite Eq.(4.10) as

$$H_\theta = \sum_{\mathrm{i}=0}^{2^{n_a}-1} \beta_{\mathrm{i}} V_{\mathrm{i}}, \tag{4.11}$$

where $n_a = \lceil \log_2 L \rceil$. The coefficient β_{i} and the operator V_{i} are determined in the following ways,

$$\begin{aligned} \beta_{\mathrm{i}} = |c_{\mathrm{i}}|, V_{\mathrm{i}} = \frac{c_{\mathrm{i}}}{|c_{\mathrm{i}}|} P_{\mathrm{i}}, \quad \text{when i} < L, \\ \beta_{\mathrm{i}} = 0, V_{\mathrm{i}} = I, \quad \text{when i} \geq L. \end{aligned} \tag{4.12}$$

4.3 Direct Measurement Method

The Direct Measurement method is inspired by the direct application of the Phase Estimation Algorithm [28] as briefly discussed in our previous publication[34]. Here the basic idea is to apply the complex-rotated Hamiltonian on the state of the molecule system and obtain the complex energy information from the output state. Since the original non-hermitian Hamiltonian can not be directly implemented in a quantum circuit, this Direct Measurement method embeds it into a larger dimensional unitary operator.

Assuming n spin orbitals needs to be considered for the system, the Direct Measurement method requires $n_s = n$ qubits to prepare the state of the model system $|\phi_r\rangle_s$ and an extra n_a ancila qubits to enlarge the non-Hermitian Hamiltonian to be a unitary operator. The quantum circuit is shown in FIG. 4.1. The B and V gates in the circuit are designed to have

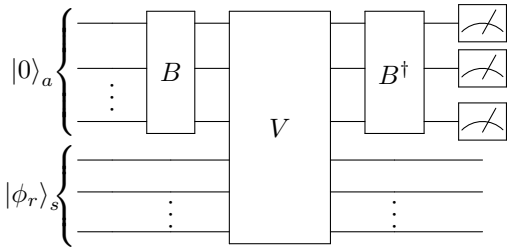

Figure 4.1. The quantum circuit for Direct Measurement method. B and V gates are constructed based on the coefficients and operators in Eq.(4.11). The system qubits' state and ancila qubits' state are initialized as $|0\rangle_a$ and $|\phi_r\rangle_s$ respectively.

the following properties

$$B|0\rangle_a = \sum_{\mathrm{i}=0}^{2^{n_a}-1} \sqrt{\frac{\beta_\mathrm{i}}{A}} |\mathrm{i}\rangle_a, A = \sum_{\mathrm{i}=0}^{2^{n_a}-1} \beta_\mathrm{i} \tag{4.13}$$

$$V|\mathrm{i}\rangle_a |\phi_r\rangle_s = |\mathrm{i}\rangle_a V_\mathrm{i} |\phi_r\rangle_s, \tag{4.14}$$

which means B transforms initial ancilla qubits' state to a vector of coefficients and V applies all V_i on system qubits based on ancilla qubits' states. One actual construction choice for B could be implementing the unitary operator

$$B = 2(\sum_{\mathrm{i}=0}^{2^{n_a}-1} \sqrt{\frac{\beta_\mathrm{i}}{A}} |\mathrm{i}\rangle_a)(\sum_{\mathrm{i}=0}^{2^{n_a}-1} \sqrt{\frac{\beta_\mathrm{i}}{A}} \langle\mathrm{i}|_a) - I. \tag{4.15}$$

As for V, a series of multi-controlled V_i gates will do the work. If $|\phi_r\rangle_s$ is chosen as an eigenstate and we apply the whole circuit of B, V and $B^\dagger$

$$U_r = (B^\dagger \otimes I^{\otimes n_s}) V (B \otimes I^{\otimes n_s}), \tag{4.16}$$

on it, the output state will be

$$U_r |0\rangle_a |\phi\rangle_s = \frac{E e^{\mathrm{i}\varphi}}{A} |0\rangle_a |\phi\rangle_s + |\Phi^\perp\rangle, \tag{4.17}$$

where $Ee^{i\varphi}$ ($E \geq 0$) is the corresponding eigenvalue and $|\Phi^{\perp}\rangle$ is a state whose ancilla qubits' state is perpendicular to $|0\rangle_a$. By measuring the output state many times, we can get $|E|$ from its relation with the possibility of the $|0\rangle_a$ state, p,

$$p = \frac{E^2}{A^2}. \tag{4.18}$$

To obtain the phase, one way is that we apply a similar circuit for $H_\theta = xI^{\otimes n} + H_\theta$, where x is a selected real number. Then the updated U_r leads us to

$$p = \frac{|x + Ee^{i\varphi}|^2}{A^2} \tag{4.19}$$

Combining with Eq. (4.18) and Eq. (4.19), we can solve the complex eigenvalue as

$$Ee^{i\varphi} = \sqrt{p}Ae^{i\cos^{-1}\frac{pA^2-x^2-pA^2}{2xA\sqrt{p}}} or \sqrt{p}Ae^{-i\cos^{-1}\frac{pA^2-x^2-pA^2}{2xA\sqrt{p}}}. \tag{4.20}$$

There are also other choices to obtain the phase. For example, instead of adding the $I^{\otimes n}$ part, we can try building the U_r based on $H_\theta + H_\theta^2$ or $H_\theta + H_\theta^3$ to get an equation like Eq.(4.19) containing phase information. That equation together with Eq.(4.18) will reveal the complex eigenvalue for the input eigenstate with another expression.

4.4 Quantum simulation of resonances in a simple model system

In this section, we will calculate the resonance properties of a model system using the Direct measurement method. This system is the following one-dimensional potential[65]

$$V(x) = (\frac{1}{2}x^2 - J)e^{-\lambda x^2} + J, \tag{4.21}$$

and parameters are chosen as $\lambda = 0.1$, $J = 0.8$. The potential is plotted in FIG. 4.2. This potential is used to model some resonance phenomena in diatomic molecules. Only

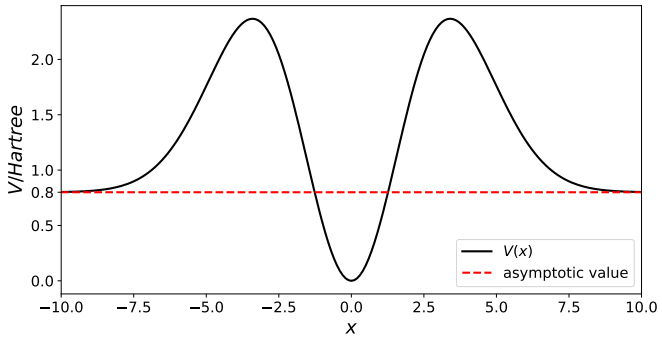

Figure 4.2. The one-dimensional potential $V(x) = (\frac{1}{2}x^2 - J)\mathrm{e}^{-\lambda x^2} + J$, where $\lambda = 0.1,\ J = 0.8$.

one electron is considered moving under this potential. The original Hamiltonian and the complex-rotated Hamiltonian can be written as

$$H = -\frac{\nabla^2}{2} + V(x), \tag{4.22}$$

$$H_\theta = -\eta^2 \frac{\nabla_x^2}{2} + V(\eta x) \tag{4.23}$$

To make the setting consistent with the original literature, η is chosen to be $\mathrm{e}^{-\mathrm{i}\theta}$ and the scaling parameter α is embed in n Gaussian basis functions

$$\chi_k(\alpha) = \exp(-\alpha_k x^2), \tag{4.24}$$

$$\alpha_k = \alpha(0.45)^k, k = 0, 1, .., n-1. \tag{4.25}$$

The $\{\chi_k(\alpha)\}$ basis set is not orthogonal, so we apply Gram-Schmidt process and iteratively construct an orthogonal basis set $\{\psi_\mathrm{i}\}$ as follows:

$$\gamma_k = \chi_k - \sum_{\mathrm{i}=0}^{k-1} \langle \chi_k | \psi_\mathrm{i} \rangle \, \psi_\mathrm{i}, \tag{4.26}$$

$$\psi_\mathrm{i} = \frac{\gamma_k}{||\gamma_k||} = \frac{\gamma_k}{\sqrt{\langle \gamma_k | \gamma_k \rangle}}. \tag{4.27}$$

Since there is only one electron, spins are not considered. This $\{\psi_{\mathrm{i}}\}$ basis set is used in the second quantization step to get the final Hamiltonian in Pauli matrix form.

The resonance eigenvalue found in [65] with $n = 10$ basis functions is

$$E_\theta = 2.124 - 0.019\mathrm{i} \quad Hartree \tag{4.28}$$

We will try to get the same resonance by applying the Direct Measurement method using the Qiskit package. The Qiskit package supports different backends, including a statevector simulator that executes circuit ideally, a QASM simulator that provides noisy gate simulation, and different IBM real quantum computers. In the following, we show the results based on the basis function number is $n = 5$ and $n = 2$. In particular, the former $n = 5$ case shows how θ trajectories locate the best resonance estimate, and the latter $n = 2$ case shows how to simplify the quantum circuit for the Direct Measurement method and run it in real IBM quantum computers.

4.4.1 n = 5

An example of the complex-rotated Hamiltonian when $n = 5$ is shown in Appendix B.1. 5 ancilla qubits and 5 system qubits are needed in this case. By choosing different scaling parameters α, the statevector simulator shows θ trajectories as FIG. 4.3. It can be seen that most trajectories pause around the point,

$$E_\theta = 2.1265 - 0.0203\mathrm{i} \quad Hartree, \tag{4.29}$$

when $\alpha = 0.65$, $\theta = 0.160$. Based on Eq.(4.1), this indicates the resonance energy and width are $E = 2.1265$ Hartree, $\Gamma = 0.0406$ Hartree, very close to the resonance energy from [65]. We also run the QASM simulator for $4 * 10^4$ shots and get the system's resonance energy at $\alpha = 0.65$, $\theta = 0.160$,

$$E_\theta = 2.1005 - 0.3862\mathrm{i} \quad Hartree. \tag{4.30}$$

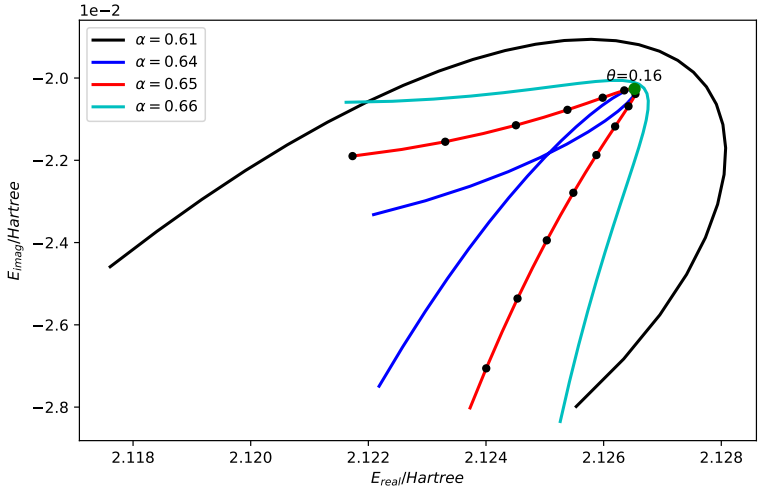

Figure 4.3. Trajectories of a complex eigenvalue on the rotation angle θ for fixed $n = 5$ and various α, calculated by Qiskit statevector simulator. θ ranges from 0.1 to 0.24 with a step of 0.01. The green point shows the best estimation of resonance energy, which is $E = 2.1265 - 0.0203$i Hartree, occurs at $\alpha = 0.65, \theta = 0.160$. The input state for the Direct Measurement method is obtained from directly diagonalizing the complex-rotated Hamiltonian matrix.

This result has an error of around 0.3 Hartree but can be augmented by more sample measurements. The real IBM quantum computer is not feasible to run the method in this size, due to the large number of standard gates in circuit.

4.4.2 n = 2

When taking $n = 2$ basis function, we are not able to locate the best resonance estimate like in FIG. 4.3 based on direct diagonalization, so we only use the Direct Measurement

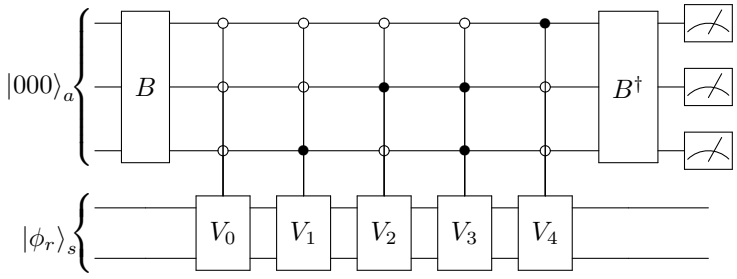

Figure 4.4. The quantum circuit to run Direct Measurement method when $n = 2$. B gate is prepared by the coefficients [1.31556, 0.13333, 0.13333, 0.25212, 1.06378]. V_0, V_1, V_2, V_3 and V_4 are applying $\mathrm{e}^{-0.04180\mathrm{i}}II$ and $\mathrm{e}^{2.32888\mathrm{i}}YY$, $\mathrm{e}^{2.32888\mathrm{i}}XX$, $\mathrm{e}^{3.05283\mathrm{i}}ZI$ and $\mathrm{e}^{3.11093\mathrm{i}}IZ$ respectively.

method to calculate the complex eigenenergy when $\alpha = 0.65$ and $\theta = 0.160$, the best location at $n = 5$. The complex-rotated Hamiltonian of the model system becomes

$$\begin{aligned} H_\theta =&(1.31441 - 0.05497\mathrm{i})II + (-0.09167 + 0.09682\mathrm{i})YY + (-0.09167 + 0.09682\mathrm{i})XX + \\ &(-0.25113 + 0.02235\mathrm{i})ZI + (-1.06328 + 0.03261\mathrm{i})IZ \\ =&1.31556 * \mathrm{e}^{-0.04180\mathrm{i}}II + 0.13333 * \mathrm{e}^{2.32888\mathrm{i}}YY + 0.13333 * \mathrm{e}^{2.32888\mathrm{i}}XX \\ &0.25212 * \mathrm{e}^{3.05283\mathrm{i}}ZI + 1.06378 * \mathrm{e}^{3.11093\mathrm{i}}IZ. \end{aligned} \tag{4.31}$$

We run with the Direct Measurement method with simulators first and then try to reduce the number of ancilla qubits to make the resulting circuit short enough to be executed in the real IBM quantum computers.

5-qubit circuit

For the Hamiltonian H_θ in Eq.(4.31), totally 5 qubits are required to calculate the Hamiltonian with the Direct Measurement method: 2 for the system qubits and 3 for the ancila qubits. FIG. 4.4 gives the quantum circuit for H_θ. By running the circuit for H_θ and a similar circuit for $H_\theta = xII + H_\theta$, the complex eigenvalue can be derived by

$$E\mathrm{e}^{\mathrm{i}\varphi} = \sqrt{p}A\mathrm{e}^{\mathrm{i}\cos^{-1}\frac{pA^2-x^2-pA^2}{2xA\sqrt{p}}} or \sqrt{p}A\mathrm{e}^{-\mathrm{i}\cos^{-1}\frac{pA^2-x^2-pA^2}{2xA\sqrt{p}}}, \tag{4.32}$$

where A and A can be obtained from the absolute value of coefficients in H_θ and H_θ, p and p can be obtained from measurement results.

This circuit can be executed in simulators, but it is still too complicated to be successfully run in the IBM quantum computers. The simulation results are listed in TABLE. 4.1.

Table 4.1. The complex eigenenergy obtained by direct diagonalizing the Hamiltonian and by running different simulators. The QASM simulator is configured to have no noise, and it takes 10^5 samples to calculate the complex eigenenergy.

Method	Eigenenergy (Hartree)	Error (Hartree)
Direct Diagonalization	2.1259-0.1089i	-
Statevector Simulator	2.1259-0.1089i	0
QASM Simulator	2.1279-0.1100i	2×10^{-3}

4-qubit circuit

We can do simplification by only calculating the eigenvalue of the Hamiltonian in Eq. (4.31) without the II part, as

$$H_\theta = 0.13333 * \mathrm{e}^{2.32888\mathrm{i}} YY + 0.13333 * \mathrm{e}^{2.32888\mathrm{i}} XX + 0.25212 * \mathrm{e}^{3.05283\mathrm{i}} ZI + 1.06378 * \mathrm{e}^{3.11093\mathrm{i}} IZ. \tag{4.33}$$

The II part can be directly added later since it is just an identity operator. Because there are only 4 terms left, 2 ancilla qubits are enough for the method. The simplified quantum circuit is then shown in FIG. 4.5.

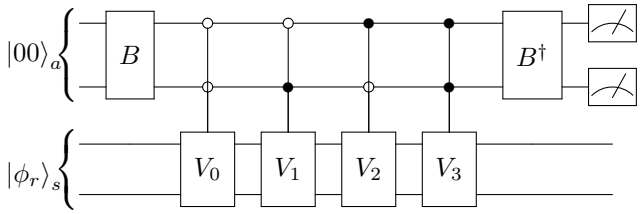

Figure 4.5. The simplified quantum circuit to run Direct Measurement method when $n = 2$. B gate is prepared by the coefficients [0.13333, 0.13333, 0.25212, 1.06378]. V_0, V_1, V_2 and V_3 are applying $\mathrm{e}^{2.32888\mathrm{i}}YY$, $\mathrm{e}^{2.32888\mathrm{i}}XX$, $\mathrm{e}^{3.05283\mathrm{i}}ZI$ and $\mathrm{e}^{3.11093\mathrm{i}}IZ$ respectively.

To avoid introducing more ancila qubits, instead of $H_\theta = H_\theta + xII$, we can run a similar 4-qubit circuit for $H_\theta = H_\theta + H_\theta^3$, which has the same terms of tensor products as H_θ with different coefficients. The complex eigenvalue can be represented by

$$E\mathrm{e}^{\mathrm{i}\varphi} = (1.31441 - 0.05497\mathrm{i}) + \sqrt{p}A\mathrm{e}^{\frac{\mathrm{i}}{2}\cos^{-1}(\frac{pA^2}{2p^2A^4} - \frac{1}{2pA^2} - \frac{pA^2}{2})} \quad \text{or} \tag{4.34}$$

$$(1.31441 - 0.05497\mathrm{i}) + \sqrt{p}A\mathrm{e}^{\frac{-\mathrm{i}}{2}\cos^{-1}(\frac{pA^2}{2p^2A^4} - \frac{1}{2pA^2} - \frac{pA^2}{2})}, \tag{4.35}$$

where A and A can be obtained from the absolute value of coefficients in H_θ and H_θ, p and p can be obtained from measurement results.

This circuit can be executed successfully in the simulators and the IBM quantum computers. However, it costs around 200 gates in the IBM quantum computers, leading to pretty large error. The result resonance eigenenergies and errors can be seen in TABLE. 4.2.

Table 4.2. The complex eigenenergy obtained by direct diagonalizing the Hamiltonian, by running simulators and by running real IBM quantum computers. The QASM simulator is configured to have no noise, and it takes 10^5 samples to calculate the complex eigenenergy. The IBM quantum computer takes 2^{13} samples.

Method	Eigenenergy (Hartree)	Error (Hartree)
Direct Diagonalization	2.1259-0.1089i	-
Statevector Simulator	2.1259-0.1089i	0
QASM Simulator	2.1264-0.1099i	1×10^{-3}
IBM Quantum Computer	2.0700-0.4890i	0.3841

3-qubit circuit

For the Hamiltonian Eq. (4.33), a more simplified circuit can be constructed if we try to calculate the complex eigenvalue of its square,

$$H_\theta^2 = (1.19013 - 0.11608\mathrm{i})II + (0.53453 - 0.02842\mathrm{i})ZZ \tag{4.36}$$

$$= 1.19577 * \mathrm{e}^{-0.09723\mathrm{i}}II + 0.53529 * \mathrm{e}^{-0.05311\mathrm{i}}ZZ \tag{4.37}$$

The quantum circuit for this H_θ^2 is showed in FIG. 4.6.

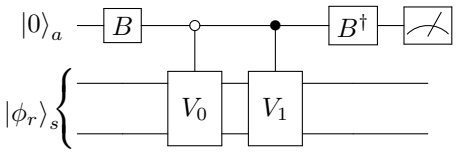

Figure 4.6. The quantum circuit to run Direct Measurement method when $n = 2$. B gate is prepared by the coefficients [1.19577, 0.53529]. V_0, V_1 are applying $\mathrm{e}^{-0.09723\mathrm{i}}II$ and $\mathrm{e}^{-0.05311\mathrm{i}}ZZ$ respectively.

We can also run a similar 3-qubit circuit for $H_\theta^2 + H_\theta^4$, which also has only 2 terms. The wanted complex eigenvalue for H_θ is

$$Ee^{i\varphi} = (1.31441 - 0.05497i) + p^{\frac{1}{4}}\sqrt{A}e^{\frac{i}{2}\cos^{-1}(\frac{pA^2}{2p^{\frac{3}{2}}A^3} - \frac{1}{2\sqrt{p}A} - \frac{\sqrt{p}A}{2})} \quad \text{or} \tag{4.38}$$

$$(1.31441 - 0.05497i) + p^{\frac{1}{4}}\sqrt{A}e^{\frac{-i}{2}\cos^{-1}(\frac{pA^2}{2p^{\frac{3}{2}}A^3} - \frac{1}{2\sqrt{p}A} - \frac{\sqrt{p}A}{2})} \tag{4.39}$$

where A and A can be obtained from the absolute value of coefficients in H_θ^2 and $H_\theta^2 + H_\theta^4$, p and p can be obtained from their measurement results.

The implementation of the circuit will cost 9 gates in the IBM quantum computers after circuit optimization. The resulting eigenenergies can be seen in TABLE. 4.3.

Table 4.3. The complex eigenenergy obtained by direct diagonalizing the Hamiltonian, by running simulators and by running real IBM quantum computers. The QASM simulator is configured to have no noise, and it takes 10^5 samples to calculate the complex eigenenergy. The IBM quantum computer takes 2^{13} samples. The error of the IBM quantum computer is from the best case.

Method	Eigenenergy (Hartree)	Error (Hartree)
Direct Diagonalization	2.1259-0.1089i	-
Statevector Simulator	2.1259-0.1089i	0
QASM Simulator	2.1259-0.1107i	1.7×10^{-3}
IBM Quantum Computer	2.1624-0.1188i	0.0378

4.5 Quantum simulation of the resonances in H_2^- using the complex scaling method

In this section, we present a proof of concept that using quantum algorithm, the Direct Measurement method, one can calculate molecular resonances on a quantum computer. Here, we focus on the resonances of the simple diatomic molecule, H_2^- $^2\Sigma_u^+(\sigma_g^2\sigma_u)$.

Moiseyev and Corcoran [64] show how to obtain the resonances of H_2^- using the variational method based on the (5s,3p,1d/3s,2p,1d) contracted Gaussian atomic basis, which

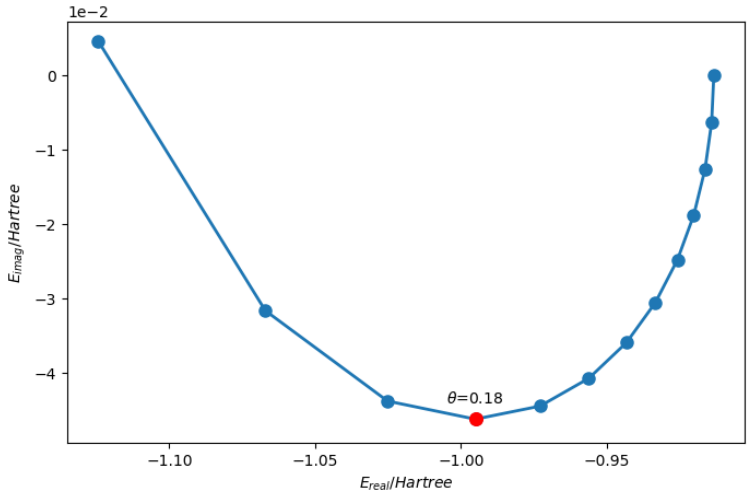

Figure 4.7. The trajectory of a complex eigenvalue on the rotation angle θ at $\alpha = 1$, calculated by a self-defined simulator. θ ranges from 0.00 to 0.24 with a step of 0.02. At the lowest point when $\theta = 0.18$, the complex eigenvalue is $-0.995102 - 0.046236$i Hartree.

contains 76 spin orbitals. The size of this basis set is too large for our method to be executed by current quantum computers or simulated by classical computers. To perform the simulation, we used the Born-Oppenheimer approximation, followed by complex rotation as shown in Section II, "COMPLEX SCALED HAMILTONIAN" and mapped to qubit space as shown in the Appendix C. We choose a much smaller 6-31g basis set for H_2^- and orthogonalize them using the Hartree-Fock method, which at the end has only a total of 8 spin orbitals.

The θ trajectory for a complex eigenvalue when $\alpha = 1.00$ is given in FIG. 4.7. If we fix $\eta = \alpha e^{-i\theta}$ at the lowest point in the figure, which has $\alpha = 1$, $\theta = 0.18$, the resonance energy obtained by the Direct Measurement method using a 16-qubit simulator is $E_\theta = -0.995102 - 0.046236$i Hartree. This complex energy is close to the one obtained by a larger basis set of 38 spin orbitals, $E_\theta = -1.0995 - 0.0432$i Hartree [64], especially the imaginary part. However, we can also see that the lowest point in the trajectory is not a good pause point. Also, in such a small basis set, we cannot find a consistent pause in different α's θ trajectories to locate the best resonance estimation. The reason for the above may be the small basis set used in the quantum simulations. However, this application gives a proof of concept and show that one can calculate molecular resonances on a quantum computer.

4.6 Conclusion

Recently, we have made progress in developing quantum simulation methods in various fields of atomic and molecular physics[1], [16], [34], [50], [66]. In this chapter, we extend the quantum simulation methods to the field of atomic and molecular resonances.

Since resonances are associated with a Hermitian Hamiltonian's complex eigenvalues, they cannot be solved directly. Here we leverage the complex rotation method to derive a non-Hermitian complex-scaled Hamiltonian. We introduce the Direct Measurement method to embed the Hamiltonian into quantum circuit. By measuring the output state multiple times, we are able to calculate complex eigenvalues from the measurement results. The new Hamiltonian's complex eigenvalues reveal to us resonances' energies and widths.

From the mathematical derivations and simulation results, it can be concluded that the Direct Measurement method can be successfully used to calculate complex eigenvalues of non-Hermitian Hamiltonians. The application on the simple one-dimensional system exhibits accurate shape resonances compared with [65] when using simulators. Although the IBM real quantum computers are not able to run large enough system size to located resonances, it still shows the effectiveness of complex eigenvalue calculation. Also, when dealing with real molecule system H_2^-, our Direct Measurement method shows a proof of concept that the systems' resonances can be calculated.

In terms of gate complexity, the Direct Measurement requires $O(n^5)$ standard gates, where n is the size of the basis set. This performs much better when compared with the exponential time complexity in traditional matrix-vector multiplication process.

Due to the time consuming simulation process, we only use up to 10 qubits to do simulation on the simple model system, and up to 8 qubits for H_2^-. This leads to errors compared with literature using a much larger basis set. It can be anticipated that once quantum computers have more available qubits and less noise, the Direct Measurement method will do a better job, more complicated molecular resonances will be revealed with more accuracy.

REFERENCES

[1] S. Kais, *Quantum Information and Computation for Chemistry: Advances in Chemical Physics*. NJ, US.: Wiley Online Library, 2014, vol. 154, p. 224 109.

[2] D. R. Herschbach, J. S. Avery, and O. Goscinski, *Dimensional scaling in chemical physics*. Springer Science & Business Media, 2012.

[3] F. Iachello and R. D. Levine, *Algebraic theory of molecules*. Oxford University Press, 1995.

[4] A. Szabo and N. S. Ostlund, *Modern quantum chemistry: introduction to advanced electronic structure theory*. Courier Corporation, 2012.

[5] J. D. Whitfield, P. J. Love, and A. Aspuru-Guzik, "Computational complexity in electronic structure," *Physical Chemistry Chemical Physics*, vol. 15, no. 2, pp. 397–411, 2013.

[6] N. Schuch and F. Verstraete, "Computational complexity of interacting electrons and fundamental limitations of density functional theory," *Nature Physics*, vol. 5, no. 10, pp. 732–735, 2009.

[7] J. D. Whitfield and Z. Zimborás, "On the np-completeness of the hartree-fock method for translationally invariant systems," *The Journal of chemical physics*, vol. 141, no. 23, p. 234 103, 2014.

[8] M. A. Nielsen and I. Chuang, *Quantum computation and quantum information*, 2002.

[9] D. S. Abrams and S. Lloyd, "Simulation of many-body fermi systems on a universal quantum computer," *Physical Review Letters*, vol. 79, no. 13, p. 2586, 1997.

[10] D. S. Abrams and S. Lloyd, "Quantum algorithm providing exponential speed increase for finding eigenvalues and eigenvectors," *Physical Review Letters*, vol. 83, no. 24, p. 5162, 1999.

[11] J. T. Seeley, M. J. Richard, and P. J. Love, "The bravyi-kitaev transformation for quantum computation of electronic structure," *The Journal of chemical physics*, vol. 137, no. 22, p. 224 109, 2012.

[12] A. Altland and B. D. Simons, *Condensed matter field theory*. Cambridge university press, 2010.

[13] P. Jordan and E. P. Wigner, "About the pauli exclusion principle," *Z. Phys.*, vol. 47, pp. 631–651, 1928.

[14] S. B. Bravyi and A. Y. Kitaev, "Fermionic quantum computation," *Annals of Physics*, vol. 298, no. 1, pp. 210–226, 2002.

[15] R. P. Feynman, "Simulating physics with computers," *International journal of theoretical physics*, vol. 21, no. 6, pp. 467–488, 1982.

[16] R. Xia, T. Bian, and S. Kais, "Electronic structure calculations and the ising hamiltonian," *The Journal of Physical Chemistry B*, 2017.

[17] M. Troyer and U.-J. Wiese, "Computational complexity and fundamental limitations to fermionic quantum monte carlo simulations," *Physical review letters*, vol. 94, no. 17, p. 170 201, 2005.

[18] S. Lloyd *et al.*, "Universal quantum simulators," *SCIENCE-NEW YORK THEN WASHINGTON-*, pp. 1073–1077, 1996.

[19] A. Aspuru-Guzik, A. D. Dutoi, P. J. Love, and M. Head-Gordon, "Simulated quantum computation of molecular energies," *Science*, vol. 309, no. 5741, pp. 1704–1707, 2005.

[20] J. D. Whitfield, J. Biamonte, and A. Aspuru-Guzik, "Simulation of electronic structure hamiltonians using quantum computers," *Molecular Physics*, vol. 109, no. 5, pp. 735–750, 2011.

[21] D. Wecker, B. Bauer, B. K. Clark, M. B. Hastings, and M. Troyer, "Gate-count estimates for performing quantum chemistry on small quantum computers," *Physical Review A*, vol. 90, no. 2, p. 022 305, 2014.

[22] H. F. Trotter, "On the product of semi-groups of operators," *Proceedings of the American Mathematical Society*, vol. 10, no. 4, pp. 545–551, 1959.

[23] M. Suzuki, "Generalized trotter's formula and systematic approximants of exponential operators and inner derivations with applications to many-body problems," *Communications in Mathematical Physics*, vol. 51, no. 2, pp. 183–190, 1976.

[24] I. Dhand and B. C. Sanders, "Stability of the trotter–suzuki decomposition," *Journal of Physics A: Mathematical and Theoretical*, vol. 47, no. 26, p. 265 206, 2014.

[25] D. W. Berry, A. M. Childs, R. Cleve, R. Kothari, and R. D. Somma, "Simulating hamiltonian dynamics with a truncated taylor series," *Physical review letters*, vol. 114, no. 9, p. 090 502, 2015.

[26] G. H. Low and I. L. Chuang, "Hamiltonian simulation by qubitization," *arXiv preprint arXiv:1610.06546*, 2016.

[27] A. Daskin and S. Kais, "An ancilla-based quantum simulation framework for non-unitary matrices," *Quantum Information Processing*, vol. 16, no. 1, p. 33, 2017.

[28] A. Daskin and S. Kais, "Direct application of the phase estimation algorithm to find the eigenvalues of the hamiltonians," *Chemical Physics*, vol. 514, pp. 87–94, 2018.

[29] A. Daskin and S. Kais, "A generalized circuit for the hamiltonian dynamics through the truncated series," *Quantum Information Processing*, vol. 17, no. 12, p. 328, 2018.

[30] A. Peruzzo, J. McClean, P. Shadbolt, M.-H. Yung, X.-Q. Zhou, P. J. Love, A. Aspuru-Guzik, and J. L. O'brien, "A variational eigenvalue solver on a photonic quantum processor," *Nature communications*, vol. 5, p. 4213, 2014.

[31] J. R. McClean, J. Romero, R. Babbush, and A. Aspuru-Guzik, "The theory of variational hybrid quantum-classical algorithms," *New Journal of Physics*, vol. 18, no. 2, p. 023 023, 2016.

[32] P. O'Malley, R. Babbush, I. Kivlichan, J. Romero, J. McClean, R. Barends, J. Kelly, P. Roushan, A. Tranter, N. Ding, *et al.*, "Scalable quantum simulation of molecular energies," *Physical Review X*, vol. 6, no. 3, p. 031 007, 2016.

[33] A. Kandala, A. Mezzacapo, K. Temme, M. Takita, M. Brink, J. M. Chow, and J. M. Gambetta, "Hardware-efficient variational quantum eigensolver for small molecules and quantum magnets," *Nature*, vol. 549, no. 7671, p. 242, 2017.

[34] T. Bian, D. Murphy, R. Xia, A. Daskin, and S. Kais, "Quantum computing methods for electronic states of the water molecule," *Molecular Physics*, pp. 1–14, 2019.

[35] S. Bravyi, J. M. Gambetta, A. Mezzacapo, and K. Temme, "Tapering off qubits to simulate fermionic hamiltonians," *arXiv preprint arXiv:1701.08213*, 2017.

[36] A. Y. Kitaev, "Quantum measurements and the abelian stabilizer problem," *arXiv preprint quant-ph/9511026*, 1995.

[37] M. Dobšíček, G. Johansson, V. Shumeiko, and G. Wendin, "Arbitrary accuracy iterative quantum phase estimation algorithm using a single ancillary qubit: A two-qubit benchmark," *Physical Review A*, vol. 76, no. 3, p. 030 306, 2007.

[38] D. W. Berry, A. M. Childs, R. Cleve, R. Kothari, and R. D. Somma, "Exponential improvement in precision for simulating sparse hamiltonians," in *Forum of Mathematics, Sigma*, Cambridge University Press, vol. 5, 2017.

[39] A. Barenco, C. H. Bennett, R. Cleve, D. P. DiVincenzo, N. Margolus, P. Shor, T. Sleator, J. A. Smolin, and H. Weinfurter, "Elementary gates for quantum computation," *Physical review A*, vol. 52, no. 5, p. 3457, 1995.

[40] P. A. Ivanov, E. Kyoseva, and N. V. Vitanov, "Engineering of arbitrary u (n) transformations by quantum householder reflections," *Physical Review A*, vol. 74, no. 2, p. 022 323, 2006.

[41] S. S. Bullock, D. P. O'Leary, and G. K. Brennen, "Asymptotically optimal quantum circuits for d-level systems," *Physical review letters*, vol. 94, no. 23, p. 230 502, 2005.

[42] J. Urías and D. A. Quiñones, "Householder methods for quantum circuit design," *Canadian Journal of Physics*, vol. 94, no. 2, pp. 150–157, 2015.

[43] R. Babbush, N. Wiebe, J. McClean, J. McClain, H. Neven, and G. K. Chan, "Low depth quantum simulation of electronic structure," *arXiv preprint arXiv:1706.00023*, 2017.

[44] J. Colless, V. Ramasesh, D. Dahlen, M. Blok, M. Kimchi-Schwartz, J. McClean, J. Carter, W. De Jong, and I. Siddiqi, "Computation of molecular spectra on a quantum processor with an error-resilient algorithm," *Physical Review X*, vol. 8, no. 1, p. 011 021, 2018.

[45] S. Sim, J. Romero, P. D. Johnson, and A. Aspuru-Guzik, "Quantum computer simulates excited states of molecule," *Physics*, vol. 11, p. 14, 2018.

[46] A. Daskin, A. Grama, and S. Kais, "A universal quantum circuit scheme for finding complex eigenvalues," *Quantum information processing*, vol. 13, no. 2, pp. 333–353, 2014.

[47] H. Wang, L.-A. Wu, Y.-x. Liu, and F. Nori, "Measurement-based quantum phase estimation algorithm for finding eigenvalues of non-unitary matrices," *Physical Review A*, vol. 82, no. 6, p. 062 303, 2010.

[48] H. Terashima and M. Ueda, "Nonunitary quantum circuit," *International Journal of Quantum Information*, vol. 3, no. 04, pp. 633–647, 2005.

[49] J. Romero, R. Babbush, J. R. McClean, C. Hempel, P. J. Love, and A. Aspuru-Guzik, "Strategies for quantum computing molecular energies using the unitary coupled cluster ansatz," *Quantum Science and Technology*, vol. 4, no. 1, p. 014 008, 2018.

[50] A. Daskin, T. Bian, R. Xia, and S. Kais, "Context aware quantum simulation of a matrix stored in quantum memory," *arXiv preprint arXiv:1904.01259*, 2019.

[51] H. Abraham, I. Y. Akhalwaya, G. Aleksandrowicz, T. Alexander, G. Alexandrowics, E. Arbel, A. Asfaw, C. Azaustre, P. Barkoutsos, G. Barron, L. Bello, Y. Ben-Haim, L. S. Bishop, S. Bosch, D. Bucher, CZ, F. Cabrera, P. Calpin, L. Capelluto, J. Carballo, C.-F. Chen, A. Chen, R. Chen, J. M. Chow, C. Claus, A. W. Cross, A. J. Cross, J. Cruz-Benito, Cryoris, C. Culver, A. D. Córcoles-Gonzales, S. Dague, M. Dartiailh,

A. R. Davila, D. Ding, E. Dumitrescu, K. Dumon, I. Duran, P. Eendebak, D. Egger, M. Everitt, P. M. Fernández, A. Frisch, A. Fuhrer, J. Gacon, Gadi, B. G. Gago, J. M. Gambetta, L. Garcia, S. Garion, Gawel-Kus, L. Gil, J. Gomez-Mosquera, S. de la Puente González, D. Greenberg, J. A. Gunnels, I. Haide, I. Hamamura, V. Havlicek, J. Hellmers, Ł. Herok, H. Horii, C. Howington, W. Hu, S. Hu, H. Imai, T. Imamichi, R. Iten, T. Itoko, A. Javadi-Abhari, Jessica, K. Johns, N. Kanazawa, A. Karazeev, P. Kassebaum, V. Krishnan, K. Krsulich, G. Kus, R. LaRose, R. Lambert, J. Latone, S. Lawrence, P. Liu, P. B. Z. Mac, Y. Maeng, A. Malyshev, J. Marecek, M. Marques, D. Mathews, A. Matsuo, D. T. McClure, C. McGarry, D. McKay, S. Meesala, A. Mezzacapo, R. Midha, Z. Minev, R. Morales, P. Murali, J. Müggenburg, D. Nadlinger, G. Nannicini, P. Nation, Y. Naveh, Nick-Singstock, P. Niroula, H. Norlen, L. J. O'Riordan, P. Ollitrault, S. Oud, D. Padilha, H. Paik, S. Perriello, A. Phan, M. Pistoia, A. Pozas-iKerstjens, V. Prutyanov, J. Pérez, Quintiii, R. Raymond, R. M.-C. Redondo, M. Reuter, D. M. Rodríguez, M. Ryu, M. Sandberg, N. Sathaye, B. Schmitt, C. Schnabel, T. L. Scholten, E. Schoute, I. F. Sertage, Y. Shi, A. Silva, Y. Siraichi, S. Sivarajah, J. A. Smolin, M. Soeken, D. Steenken, M. Stypulkoski, H. Takahashi, C. Taylor, P. Taylour, S. Thomas, M. Tillet, M. Tod, E. de la Torre, K. Trabing, M. Treinish, TrishaPe, W. Turner, Y. Vaknin, C. R. Valcarce, F. Varchon, D. Vogt-Lee, C. Vuillot, J. Weaver, R. Wieczorek, J. A. Wildstrom, R. Wille, E. Winston, J. J. Woehr, S. Woerner, R. Woo, C. J. Wood, R. Wood, S. Wood, J. Wootton, D. Yeralin, J. Yu, L. Zdanski, Zoufalc, anedumla, azulehner, bcamorrison, drholmie, fanizzamarco, kanejess, klinvill, merav-aharoni, ordmoj, tigerjack, yang.luh, and yotamvakninibm, *Qiskit: An open-source framework for quantum computing*, 2019. DOI: 10.5281/zenodo.2562110.

[52] N. Moiseyev, *Non-Hermitian quantum mechanics*. Cambridge University Press, 2011.

[53] W. P. Reinhardt, "Complex coordinates in the theory of atomic and molecular structure and dynamics," *Annual Review of Physical Chemistry*, vol. 33, no. 1, pp. 223–255, 1982.

[54] J. Aguilar and J.-M. Combes, "A class of analytic perturbations for one-body schrödinger hamiltonians," *Communications in Mathematical Physics*, vol. 22, no. 4, pp. 269–279, 1971.

[55] E. Balslev and J.-M. Combes, "Spectral properties of many-body schrödinger operators with dilatation-analytic interactions," *Communications in Mathematical Physics*, vol. 22, no. 4, pp. 280–294, 1971.

[56] B. Simon, "Quadratic form techniques and the balslev-combes theorem," *Communications in Mathematical Physics*, vol. 27, no. 1, pp. 1–9, 1972.

[57] B. Simon, "Resonances in n-body quantum systems with dilatation analytic potentials and the foundations of time-dependent perturbation theory," *Annals of Mathematics*, pp. 247–274, 1973.

[58] C. van Winter, "Complex dynamical variables for multiparticle systems with analytic interactions. i," *Journal of Mathematical Analysis and Applications*, vol. 47, no. 3, pp. 633–670, 1974.

[59] N. Moiseyev, "Quantum theory of resonances: Calculating energies, widths and cross-sections by complex scaling," *Physics reports*, vol. 302, no. 5-6, pp. 212–293, 1998.

[60] G. Doolen, "A procedure for calculating resonance eigenvalues," *Journal of Physics B: Atomic and Molecular Physics*, vol. 8, no. 4, p. 525, 1975.

[61] S. Kais and D. Herschbach, "Dimensional scaling for quasistationary states," *The Journal of chemical physics*, vol. 98, no. 5, pp. 3990–3998, 1993.

[62] T. C. Germann and S. Kais, "Large order dimensional perturbation theory for complex energy eigenvalues," *The Journal of chemical physics*, vol. 99, no. 10, pp. 7739–7747, 1993.

[63] N. Moiseyev, P. Certain, and F. Weinhold, "Complex-coordinate studies of helium autoionizing resonances," *International Journal of Quantum Chemistry*, vol. 14, no. 6, pp. 727–736, 1978.

[64] N. Moiseyev and C. Corcoran, "Autoionizing states of h 2 and h 2- using the complex-scaling method," *Physical Review A*, vol. 20, no. 3, p. 814, 1979.

[65] N. Moiseyev, P. Certain, and F. Weinhold, "Resonance properties of complex-rotated hamiltonians," *Molecular Physics*, vol. 36, no. 6, pp. 1613–1630, 1978.

[66] R. Xia and S. Kais, "Quantum machine learning for electronic structure calculations," *Nature communications*, vol. 9, no. 1, pp. 1–6, 2018.

A. H_2O HAMILTONIAN AT EQUILIBRIUM

Table A.1. Pauli matrix form Hamiltonian for the water molecule at equilibrium when O-H is 1.9 a.u. There are 95 terms, and listed are each operator and corresponding coefficient. X, Y, Z, I stand for the spin matrices $\sigma^x, \sigma^y, \sigma^z$ and the identity operator on a single qubit subspace.

IIIIII	-72.008089	IIIIIZ	0.373979	IIIIXX	-0.050755
IIIIYY	0.113535	IIIIZI	0.002526	IIIIZZ	0.779273
IIIZII	-0.771553	IIIZIZ	0.043092	IIIZXX	0.113535
IIIZYY	-0.050755	IIIZZI	0.785287	IIIZZZ	-0.030367
IIXIIX	0.009295	IIXIXI	0.000158	IIXIZX	-0.009295
IIXZXZ	-0.000158	IIZIII	-0.373979	IIZIIZ	-0.148141
IIZIYY	-0.011744	IIZIZZ	-0.146285	IIZZII	0.141059
IIZZXX	-0.011744	IIZZZI	-0.136887	IXIIIX	0.000158
IXIIXI	0.013400	IXIIZX	-0.000158	IXIZXZ	-0.013400
IXXIII	-0.050755	IYYIII	0.113535	IYYIIZ	0.011744
IYYIYY	0.019371	IYYIZZ	0.031747	IYYZII	-0.011216
IYYZXX	0.019371	IYYZZI	0.031561	IZIIII	-0.002526
IZXIIX	0.009295	IZXIXI	0.000158	IZXIZX	-0.009295
IZXZXZ	-0.000158	IZZIII	0.779273	IZZIIZ	0.146285
IZZIYY	0.031747	IZZIZZ	0.220040	IZZZII	-0.154863
IZZZXX	0.031747	IZZZZI	0.179396	XIIXII	0.012412
XIIXXX	-0.007950	XIIXZI	0.012412	XIIYXY	0.007950
XXXXII	-0.007950	XXXXXX	0.018156	XXXXZI	-0.007950
XXXYXY	-0.018156	XXZXXZ	-0.006979	XXZYYI	0.006979
XZIXII	-0.012412	XZIXXX	0.007950	XZIXZI	-0.012412
XZIYXY	-0.007950	YXYXII	0.007950	YXYXXX	-0.018156
YXYXZI	0.007950	YXYYXY	0.018156	YYIXXZ	-0.006979
YYIYYI	0.006979	ZIIIII	0.771553	ZIIIIZ	0.141059
ZIIIYY	0.011216	ZIIIZZ	0.154863	ZIIZII	-0.154860
ZIIZXX	0.011216	ZIIZZI	0.146877	ZIZIII	0.043092
ZXXIII	-0.113535	ZXXIIZ	-0.011744	ZXXIYY	-0.019371
ZXXIZZ	-0.031747	ZXXZII	0.011216	ZXXZXX	-0.019371
ZXXZZI	-0.031561	ZXZIIX	-0.000158	ZXZIXI	-0.013400
ZXZIZX	0.000158	ZXZZXZ	0.013400	ZYYIII	0.050755
ZZIIII	0.785287	ZZIIIZ	0.136887	ZZIIYY	0.031561
ZZIIZZ	0.179396	ZZIZII	-0.146877	ZZIZXX	0.031561
ZZIZZI	0.189343	ZZZIII	0.030367		

B. COMPLEX-ROTATED HAMILTONIAN OF THE MODEL SYSTEM AT $\theta = 0.16$, $\alpha = 0.65$ WHEN $n = 5$

Table B.1. The coefficients and tensor product operators of complex-rotated Hamiltonian H_θ at $\theta = 0.16$, $\alpha = 0.65$ when there are $n = 5$ basis functions.

YYIII	-0.091665+0.096819i	XXIII	-0.091665+0.096819i
IIIII	4.599205-0.533073i	ZIIII	-0.251131+0.022353i
YZYII	0.0179156-0.030997i	XZXII	0.0179156-0.030997i
YZZYI	-0.007005+0.015446i	XZZXI	-0.007005+0.015446i
YZZZY	0.003680-0.009152i	XZZZX	0.003680-0.009152i
IZIII	-1.063280+0.032614i	IYYII	-0.089297+0.108259i
IXXII	-0.089297+0.108259i	IYZYI	0.014213-0.055870i
IXZXI	0.014213-0.055870i	IYZZY	-0.003869+0.033693i
IXZZX	-0.003869+0.033693i	IIZII	-1.445349+0.113618i
IIYYI	-0.209952+0.010748i	IIXXI	-0.209952+0.010748i
IIYZY	0.060302-0.008776j	IIXZX	0.060302-0.008776i
IIIZI	-1.127058+0.243702i	IIIYY	-0.336956+0.051691i
IIIXX	-0.336956+0.051691i	IIIIZ	-0.712385+0.120784i

C. COMPLEX-ROTATED HAMILTONIAN OF H_2^- AT $\theta = 0.18$, $\alpha = 1.00$ USING 6-31G BASIS SET

Table C.1. The coefficients and tensor product operators in H_2^-'s complex-rotated Hamiltonian at $\theta = 0.18$, $\alpha = 1.00$ when using 6-31g basis set.

IXZXXZXI	0.018705 -0.003404i	IIIZIXZX	0.038191 -0.006950i
ZIZIIIII	0.103932 -0.018913i	XZXIXZXI	0.027826 -0.005063i
IXXIIIXX	-0.002794+0.000508i	IIZZIIII	0.106657 -0.019408i
IYIYIIII	0.024307 -0.004423i	IIIIXXXX	0.015119 -0.002751i
IZIIIIZI	0.095226 -0.017328i	IIIIIIXX	0.047512 -0.039979i
YYIIYZZY	-0.019254+0.003504i	XZXIYZYI	0.027826 -0.005063i
IZIIYZYI	0.013080 -0.002380i	IIYYIIXX	0.034554 -0.006288i
XZXIIIZI	0.032587 -0.005930i	YYYYIIII	0.015119 -0.002751i
XXIIIYYI	0.005216 -0.000949i	IXIXIIII	0.024307 -0.004423i
IIIIXXYY	0.002918 -0.000531i	IIIZXZXI	0.050249 -0.009144i
IIXXXXII	0.020481 -0.003727i	YYIIYYII	0.019597 -0.003566i
IXXIIXXI	0.008283 -0.001507i	IIIIXIXI	0.016733 -0.003045i
IYZYIIII	-0.035671+0.030324i	IYZYIIIZ	0.043018 -0.007828i
YYIIIYYI	0.005216 -0.000949i	IIIIXZZX	-0.028316+0.033738i
XXIIYYII	0.019597 -0.003566i	IXXIIIYY	-0.002794+0.000508i
ZYZYIIII	0.015436 -0.002809i	XXIIYZZY	-0.019254+0.003504i
IIIIIZZI	0.084620 -0.015398i	YZYIIZII	0.011702 -0.002129i
IIYYXZZX	-0.031698+0.005768i	IIIIIXXI	-0.007550+0.006494i
IXZXIZII	0.012371 -0.002251i	IIIIYYYY	0.015119 -0.002751i
IIIZYZYI	0.050249 -0.009144i	ZIIIIIII	-0.230405+0.108639i
ZIIIIIIZ	0.159054 -0.028943i	IXXIYZZY	0.006593 -0.001200i
IIIIIYIY	0.023153 -0.004213i	IIYYIXXI	-0.000541+0.000098i
YZZYIIII	-0.027204+0.031862i	IIIZIIZI	0.139579 -0.025399i
YZZYXXII	-0.016647+0.003029i	IIXXIIII	0.047746 -0.040370i
XIXIIIII	0.017118 -0.003115i	YYIIXXII	0.019597 -0.003566i
YZYIIYZY	0.017127 -0.003117i	IIIIZZII	0.084496 -0.015376i
YZZYXZZX	0.031161 -0.005670i	IIZIIYZY	0.024717 -0.004498i
XZZXIXXI	0.004990 -0.000908i	IYYIIYYI	0.008283 -0.001507i
IYZYIXZX	0.015728 -0.002862i	XZZXXZZX	0.031161 -0.005670i

Table C.1. (Continued) The coefficients and tensor product operators in H_2^-'s complex-rotated Hamiltonian at $\theta = 0.18$, $\alpha = 1.00$ when using 6-31g basis set.

IYZYIIZI	0.026040 -0.004739i	IIZIIZII	0.093507 -0.017015i
IZIIZIII	0.106161 -0.019318i	XXIIIXXI	0.005216 -0.000949i
IXZXIYZY	0.015728 -0.002862i	ZIIIIXZX	0.030922 -0.005627i
IIIIIIYY	0.047512 -0.039979i	XXIIIIYY	0.021209 -0.003859i
XXIIIIXX	0.021209 -0.003859i	YYIIIIII	0.001646 -0.022572i
ZIIIIIZI	0.130169 -0.023687i	IIYYIIYY	0.034554 -0.006288i
YZYIIIIZ	0.052229 -0.009504i	YZYIIIII	-0.021561+0.077956i
IIXXXZZX	-0.031698+0.005768i	IIIIZYZY	0.013729 -0.002498i
IYYIXXII	0.003919 -0.000713i	IIZIZIII	0.133407 -0.024276i
YZZYYZZY	0.031161 -0.005670i	XZXIZIII	0.040337 -0.007340i
ZIIIZIII	0.151365 -0.027544i	YZYIIXZX	0.017127 -0.003117i
IIIIYIYI	0.016733 -0.003045i	IIXXIYYI	-0.000541+0.000098i
IIYYYZZY	-0.031698+0.005768i	IYYIIIII	-0.009705+0.008779i
YZZYYYII	-0.016647+0.003029i	XZXIIXZX	0.017127 -0.003117i
IIIIIXIX	0.023153 -0.004213i	IIZIYZYI	0.033580 -0.006110i
ZXZXIIII	0.015436 -0.002809i	YZYZIIII	0.020644 -0.003757i
IIIIYZZY	-0.028316+0.033738i	IXZXZIII	0.034152 -0.006215i
YZZYIYYI	0.004990 -0.000908i	ZIIZIIII	0.126456 -0.023011i
YZZYIIXX	-0.029557+0.005379i	XZZXYZZY	0.031161 -0.005670i
IYYIIIYY	-0.002794+0.000508i	IXZXIIII	-0.035671+0.030324i
IXZXIIIZ	0.043018 -0.007828i	ZIIIYZYI	0.038659 -0.007035i
IIXXIIXX	0.034554 -0.006288i	ZZIIIIII	0.085046 -0.015476i
IIIZZIII	0.158431 -0.028830i	YXXYIIII	0.012162 -0.002213i
IZIIIYZY	0.013159 -0.002395i	IYZYXZXI	0.018705 -0.003404i
XXIIXXII	0.019597 -0.003566i	IIIIYXXY	0.012201 -0.002220i
IIIIZIII	-0.231557+0.112195i	IIIIZIIZ	0.128680 -0.023416i
YZYIXZXI	0.027826 -0.005063i	IIYYYYII	0.020481 -0.003727i
IIIIXZXZ	0.020604 -0.003749i	IIIIXZXI	-0.030067+0.081498i
IIYYIYYI	-0.000541+0.000098i	IYYIYZZY	0.006593 -0.001200i

Table C.1. (Continued) The coefficients and tensor product operators in H_2^-'s complex-rotated Hamiltonian at $\theta = 0.18$, $\alpha = 1.00$ when using 6-31g basis set.

YZYIYZYI	0.027826 -0.005063i	IIZIXZXI	0.033580 -0.006110i
IIXXYZZY	-0.031698+0.005768i	IIIIIIZI	-0.611815+0.267480i
IIIIIIZZ	0.107859 -0.019627i	YZZYIXXI	0.004990 -0.000908i
IIIIIXZX	-0.012982+0.018373i	IXXIXXII	0.003919 -0.000713i
IIZIIIII	-0.612966+0.271036i	XZXIIYZY	0.017127 -0.003117i
IIXXIXXI	-0.000541+0.000098i	IIIIYYII	0.000598 -0.021276i
YYIIIIXX	0.021209 -0.003859i	XZZXYYII	-0.016647+0.003029i
XZXZIIII	0.020644 -0.003757i	YZZYIIYY	-0.029557+0.005379i
YYXXIIII	0.002957 -0.000538i	YZYIIIZI	0.032587 -0.005930i
IIXXYYII	0.020481 -0.003727i	IXZXIXZX	0.015728 -0.002862i
IXZXIIZI	0.026040 -0.004739i	XYYXIIII	0.012162 -0.002213i
ZIIIXZXI	0.038659 -0.007035i	IIXXIIYY	0.034554 -0.006288i
YYIIIIYY	0.021209 -0.003859i	IZZIIIII	0.087497 -0.015922i
IZIIIZII	0.094105 -0.017124i	IIYYXXII	0.020481 -0.003727i
IIIZIYZY	0.038191 -0.006950i	IYYIIIXX	-0.002794+0.000508i
IXXIXZZX	0.006593 -0.001200i	IIIIZXZX	0.013729 -0.002498i
IIIIIYYI	-0.007550+0.006494i	IIIIZIZI	0.103932 -0.018913i
YYIIXZZX	-0.019254+0.003504i	IXXIIIII	-0.009705+0.008779i
IIIIXXII	0.000598 -0.021276i	XZZXIYYI	0.004990 -0.000908i
IZIIIIIZ	0.110454 -0.020099i	IZIIIIII	-0.388873+0.102313i
IYZYIZII	0.012371 -0.002251i	IXXIIYYI	0.008283 -0.001507i
IYYIYYII	0.003919 -0.000713i	YYIIIXXI	0.005216 -0.000949i
XXYYIIII	0.002957 -0.000538i	IXXIYYII	0.003919 -0.000713i
IIIIYZYZ	0.020604 -0.003749i	IIIIYZYI	-0.030067+0.081498i
IYZYIYZY	0.015728 -0.002862i	IZIIXZXI	0.013080 -0.002380i
IIIIIIII	1.734311 -1.110499i	IIIIIIIZ	-0.896247+0.369556i
IIZIIXZX	0.024717 -0.004498i	IZIIIXZX	0.013159 -0.002395i
IIZIIIZI	0.120598 -0.021945i	XZZXIIYY	-0.029557+0.005379i
IIIIXYYX	0.012201 -0.002220i	IYZYZIII	0.034152 -0.006215i

Table C.1. (Continued) The coefficients and tensor product operators in H_2^-'s complex-rotated Hamiltonian at $\theta = 0.18$, $\alpha = 1.00$ when using 6-31g basis set.

IIYYIIII	0.047746 -0.040370i	IXZXYZYI	0.018705 -0.003404i
XZXIIIIZ	0.052229 -0.009504i	XZXIIIII	-0.021561+0.077956i
XZZXXXII	-0.016647+0.003029i	ZIIIIYZY	0.030922 -0.005627i
YIYIIIII	0.017118 -0.003115i	IYYIXZZX	0.006593 -0.001200i
XZZXIIII	-0.027204+0.031862i	IIIIIYZY	-0.012982+0.018373i
XXIIXZZX	-0.019254+0.003504i	XZXIIZII	0.011702 -0.002129i
ZIIIIZII	0.102700 -0.018688i	IIIIIZIZ	0.092214 -0.016780i
IIIIIZII	-0.386698+0.100135i	IYYIIXXI	0.008283 -0.001507i
IIIZIZII	0.105681 -0.019231i	XXIIIIII	0.001646 -0.022572i
IIIIYYXX	0.002918 -0.000531i	IZIZIIII	0.092214 -0.016780i
YZYIZIII	0.040337 -0.007340i	XXXXIIII	0.015119 -0.002751i
XZZXIIXX	-0.029557+0.005379i	IIIZIIIZ	0.184425 -0.033560i
IIIZIIII	-0.894071+0.367379i	IIZIIIIZ	0.144136 -0.026228i
IYZYYZYI	0.018705 -0.003404i		

VITA

Teng Bian, born Zhuji, Zhejiang, People's Republic of China; received B.S. in Applied Physics from University of Science and Technology of China in 2015; graduate student, Purdue University, 2015 up to the present.